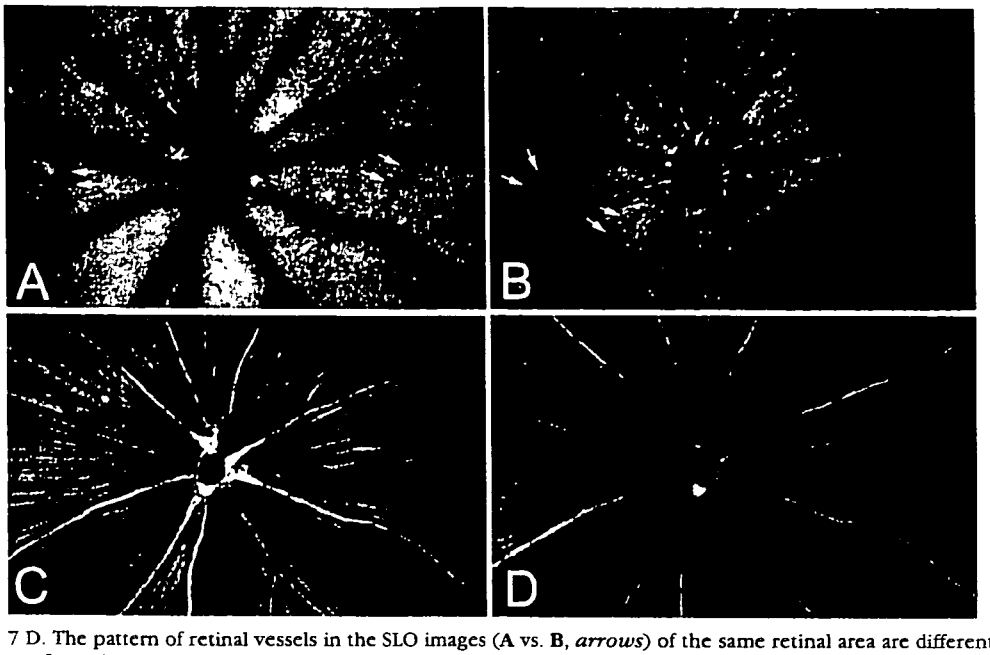

FIGURE 1. SLO images of normal rat fundus recorded under argon blue laser illumination through the narrowest confocal aperture. The focused plane was sequentially moved from sclerad (A) to vitread (D) by changing the refractive values (ΔF) in the SLO setting. (A) Refractive value, −8 D. White mottled reflex from the retinal pigment epithelium was prominent. Striations of RNFL are not visible. (B) Refractive value, −4 D. Radial striations of RNFL became visible. (C) Refractive value, +3 D. The striations of RNFL reflex were prominent. The dark area around the optic disc increased in size with larger refractive values than with this one. (D) Refractive value, +5 D. The large dark area around the optic disc indicates that the focused plane was in front of the retinal surface. In this case, the range of refractive values in which radial striations of RNFL are clearly observed near the optic disc is from −4 D to +3 D, and thus ΔF is 7 D. The pattern of retinal vessels in the SLO images (A vs. B, *arrows*) of the same retinal area are different at different focal planes, a finding that confirms the ability of the SLO for optical sectioning of rat retina using a 488-nm laser.

of 2.75 mm and a diameter of 5.0 mm (Kyoto Contact Lens, Kyoto, Japan) was placed on the cornea after topical anesthesia with 0.4% oxybuprocaine hydrochloride eye drops (Santen Pharmaceuticals). A rat was placed on a heating pad (Deltaphase Isothermal Pad; Braintree Scientific, Inc., Braintree, MA) and its head was gently held manually to keep the eye in position for illuminating the fundus evenly with the argon blue laser.

Fundus images with a field angle of 40° were recorded by digital video (GV-D1000; Sony Co., Tokyo, Japan). First, the widest confocal aperture (C3) was used for qualitative observation of RNFL. Then, for the quantitative evaluation of RNFL thickness, the narrowest confocal aperture (C1) was used to maximize the image contrast of the focused plane and the axial resolution. The focused plane was sequentially moved through the retina, sclerad to vitread, by changing the refractive values (maximum range, −20 D to +20 D) in the SLO setting (i.e., altering the setting of the ametropic corrector). The fundus images were recorded with a nominal 1-D step and the range of refractive values (ΔF) for RNFL thickness was determined by a masked observer.

As the focus measurements in this study were subjective, representative SLO images of RNFL with different focused planes, as shown in Figure 1, were used as the reference images for determining ΔF. For all 1-D steps of SLO images of each rat fundus, we looked carefully at the retinal location, approximately 1 disc diameter apart from the edges of the optic disc and determined the most sclerad focal plane where the radial striations of RNFL become just visible. We also determined the most vitread focal plane with the striations of RNFL reflex just before being covered by the dark area around the optic disc which enlarges with larger refractive values. For evaluation of the reproducibility and reliability of these subjective focus measurements, we calculated intra- and interobserver agreement in the measurements using the SLO image series of 24 rat fundi (six image series each at baseline and 1, 2, and 4 weeks after the optic nerve crush). Two observers independently determined ΔF for each rat fundus. The image series were presented in a random sequence on two separate occasions. The κ statistic was 0.92 and 0.83 for intra- and interobserver agreement respectively, indicating that reproducibility of the focus measurements was relatively good.

For each rat, we examined the fundus by indirect ophthalmoscopy after SLO imaging to ensure that visibility of the fundus was not compromised by the optic nerve crush surgery or other problems that may cause corneal opacity or cataract.

Correlation of ΔF and Histologically Determined RNFL Thickness

Sixteen rats were divided into four groups (four rats in each group). An optic nerve crush was performed in the right eye in three groups. Retinal sections of the right eye were prepared for RNFL thickness measurement at 1, 2, and 4 weeks after optic nerve crush. One group of rats was used for each time point. For baseline data, the optic nerve was not crushed in the remaining group of rats, and the right eye was processed similarly. Immediately after the recording of the fundus by SLO, the eyes were enucleated after administration of an anesthetic overdose of intraperitoneal pentobarbital sodium. The anterior segment was removed and a small marking cut was placed on the edge of the posterior eye cup to identify the superior retinal portion. The eye cup was fixed in 4% paraformaldehyde-0.5% glutaraldehyde and 0.1 M phosphate-buffered saline for 2 hours at room temperature, and was embedded in mounting compound (Tissue-TeK OCT; Sakura Finetechnical, Tokyo, Japan) followed by freezing with dry ice. Serial frozen sections (16 μm thick) were collected along the vertical meridian of the globe. After they were stained with hematoxylin-eosin, the retinal sections were observed under an optical microscope (Eclipse TE300; Nikon Corp., Kanagawa, Japan) and were recorded as JPEG files with a digital cooled CCD camera (DS-5Mc-L1; Nikon) and a personal computer (Dimension 8300; Dell Inc., Round Rock, TX). For each eye, RNFL thickness of three consecutive sections derived from a location approximately 500 μm temporal from the center of the optic disc (~1 disc diameter from the edge of the optic disc) was measured using image-analysis software (Image-Pro Express 4.0; MediaCybernetics, Inc., Silver Spring, MD) and averaged. The RNFL thickness in the retinal sections was compared by the ΔF determined from SLO images.

We also counted the number of cells in the ganglion cell layer in the retinal sections used for RNFL thickness measurements and calculated the mean number of cells in each eye.

Statistical Analysis

The difference in ΔF was analyzed by the Wilcoxon signed-rank test for comparison between control and crushed eyes and by the Friedman test and post hoc tests for comparison of ΔF measured at different time points. The differences in RNFL thickness and the number of cells in the ganglion cell layer in retinal sections at different time points were

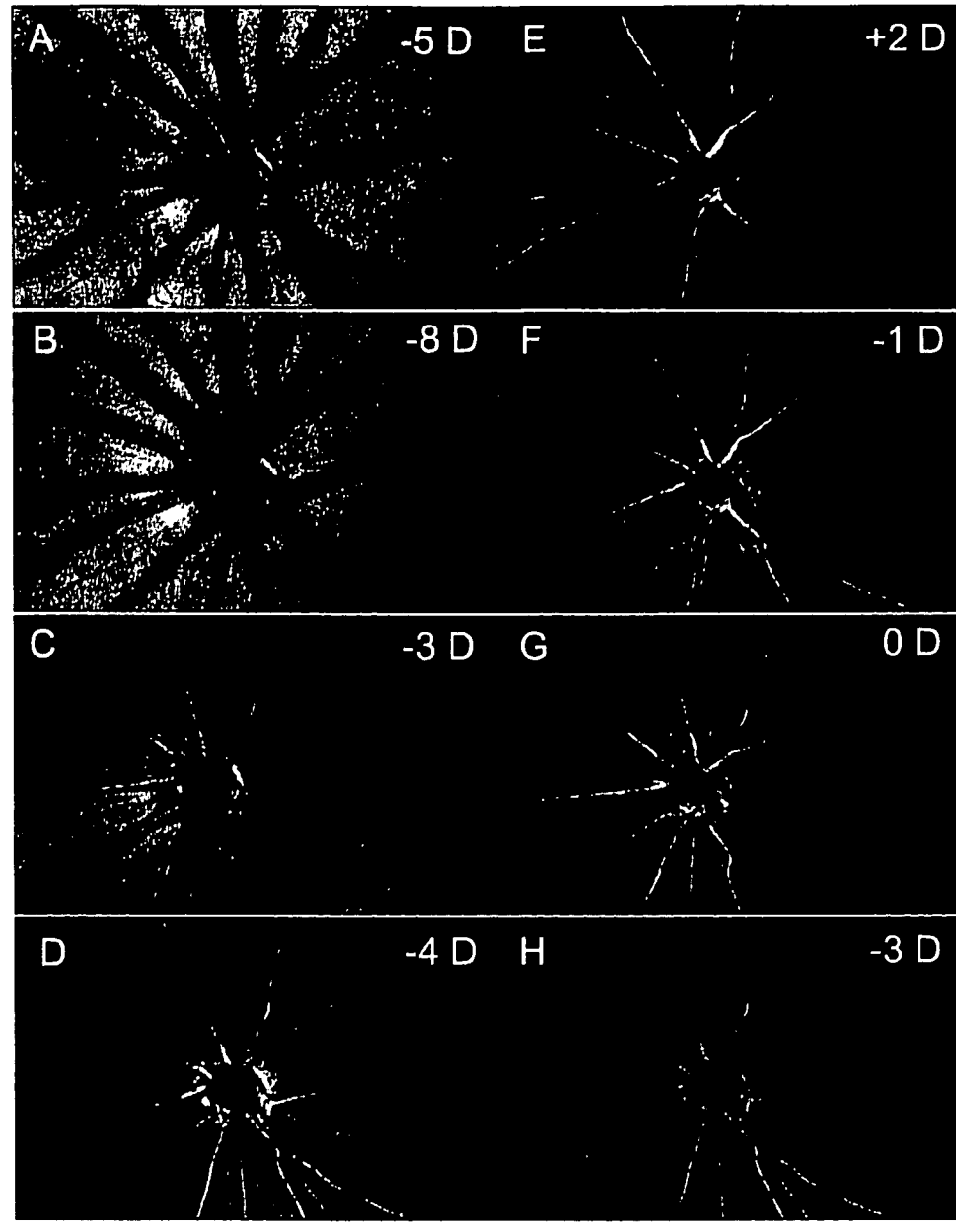

FIGURE 2. RNFL changes over time caused by optic nerve crush. SLO images at baseline (**A**, **E**) and 1 (**B**, **F**), 2 (**C**, **G**), and 4 (**D**, **H**) weeks after axonal injury. (**A**–**D**) Fundus images taken at the lower limit of refractive value for RNFL observation. (**E**–**H**) Fundus images taken at the upper limit of refractive value for RNFL observation. The refractive value of each SLO image is shown at *top right*.

analyzed by one-way ANOVA and post hoc tests. Spearman's rank-order correlation coefficient was calculated to determine the significance of the correlation between ΔF and RNFL thickness measured in retinal sections. $P < 0.05$ was considered statistically significant. Data are expressed as the mean ± SD.

RESULTS

Striations of RNFL radiating from the optic disc were clearly visible in each eye by SLO under argon blue laser illumination when appropriately focused (Fig. 1). The fundus images were sharper, but darker through a C1 than through a C3 confocal aperture (data not shown). After the optic nerve crush, no obvious changes in RNFL reflex were observed 1 week later. However, 2 weeks after the crush, striations of RNFL became uniformly darker and thinner, suggesting diffuse loss of retinal ganglion cell axons. Disappearance of RNFL striations was more evident 4 weeks after the crush (Fig. 2). The RNFL changes after the optic nerve crush were consistent in all 21 rats. In contrast, RNFL appearance of control eyes was unchanged throughout the experimental period.

For the quantitative evaluation of RNFL thickness, the range of refractive values (ΔF) in the SLO setting in which radial striations of RNFL was clearly observed near the optic disc was determined at each time point in both eyes of all 21 rats. The ΔF before and 1, 2, and 4 weeks after the optic nerve crush was 7.1 ± 0.4, 7.2 ± 0.7, 3.4 ± 0.5 and 1.2 ± 0.4 D, respectively (Fig. 3). The ΔF was unchanged 1 week after the crush, but then decreased significantly and progressively after the second week. No significant changes in ΔF were observed in the untreated control eyes during the experimental period.

To determine whether ΔF is a reliable indicator of actual RNFL thickness, the thickness was measured in frozen sections of the retina after the ΔF measurements by SLO (Fig. 4). The RNFL thickness at a location approximately 500 μm temporal from the center of the optic disc in retinal sections before and 1, 2, and 4 weeks after the optic nerve crush was 24.9 ± 2.4, 25.9 ± 3.3, 9.8 ± 1.0, and 3.9 ± 0.2 μm, respectively. The

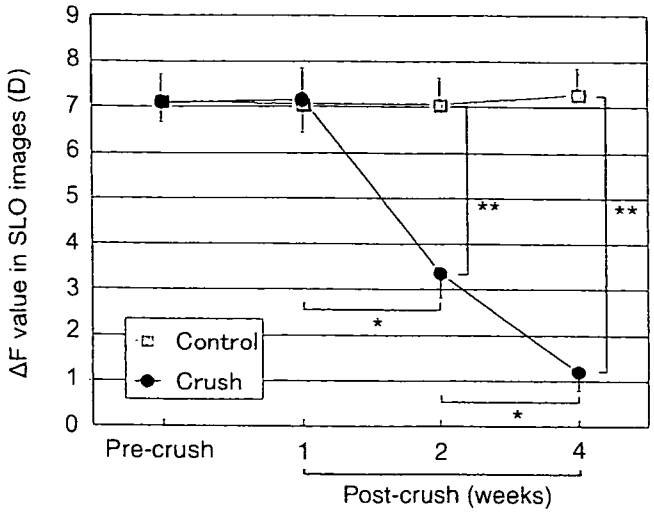

FIGURE 3. Changes of ΔF in SLO images over time caused by the optic nerve crush. Fundus images were recorded using a 1-D step and the range of refractive values (ΔF) where radial striations of RNFL were clearly observed near the optic disc was determined. Data are presented as the mean ± SD (n = 21 each). *P < 0.001 (Friedman test and post hoc tests). **P < 0.001 (Wilcoxon signed-rank test).

thickness was unchanged 1 week after the crush, but then decreased significantly and progressively after the second week. There was a significant positive relationship (r = 0.86, P < 0.001) between ΔF and the histologically determined RNFL thickness (Fig. 5). In contrast, the cell counts in the ganglion cell layer expressed as a percentage of the baseline count (100% ± 6.7%) were 73.6% ± 6.6%, 41.4% ± 2.0%, and 22.8% ± 2.4% at 1, 2, and 4 weeks after optic nerve crush, respectively. This decrease in cell count from baseline was significant 1 week after the crush and progressed further thereafter (P < 0.01).

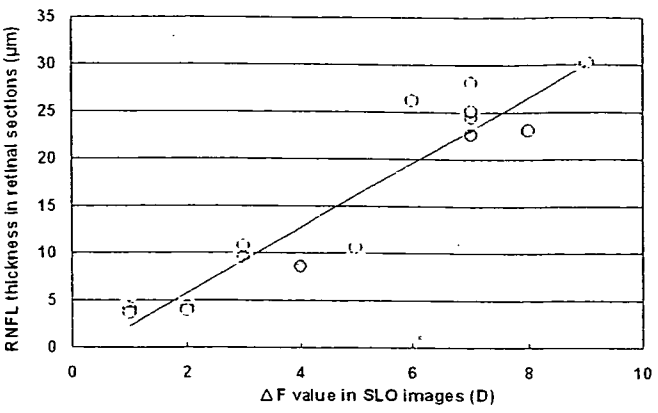

FIGURE 5. Correlation of ΔF and histologically determined RNFL thickness. Spearman's rank-order correlation coefficient analysis shows a significant positive relationship between ΔF and the histologically determined RNFL thickness (r = 0.86, P < 0.001, n = 16).

DISCUSSION

In contrast to the clinical significance of RNFL assessment for diagnosis and management of glaucoma and other optic neuropathies, there have been few reports dealing with the changes of the RNFL or intraretinal axons of retinal ganglion cells in rodent models with optic nerve injuries. An immunohistochemical study showed thick bundles of retinal ganglion cell axons converging toward the optic disc in wholemounts of normal rat retina.[6] The striations radiating from the optic disc in rat retina observed by SLO imaging under argon blue laser illumination seemed quite similar to the intraretinal distribution of retinal ganglion cell axons.[6] Given that the condition used for imaging the rat retina in this study was optimal for RNFL observation of human retina, the radial striations in SLO images were considered to be the reflex from the bundle of retinal ganglion cell axons.

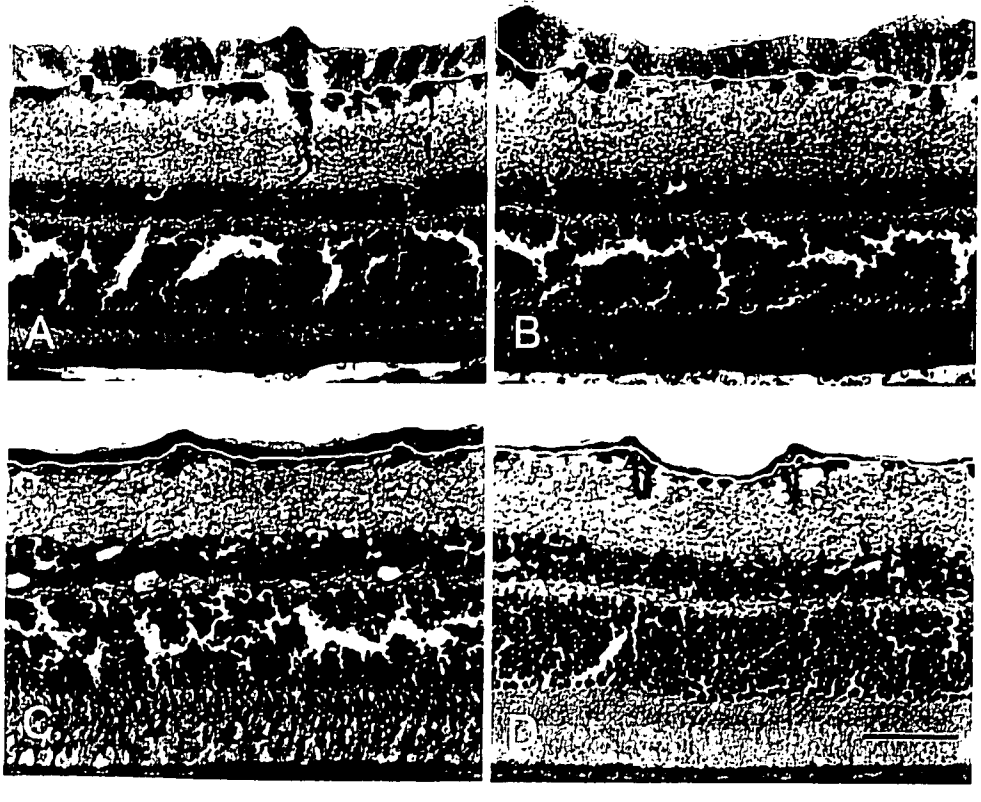

FIGURE 4. Representative photographs of retinal sections showing the changes of RNFL after the optic nerve crush. (A) Baseline and (B) 1, (C) 2, and (D) 4 weeks after axonal injury. *White line* demarcates the area of RNFL in each retinal section. The size of the RNFL area was measured with image-analysis software and the average RNFL thickness of three serial sections was determined. Scale bar, 50 μm.

The clinical usefulness of RNFL evaluation by SLO is limited because SLO evaluation of human RNFL remains qualitative. Other imaging modalities such as optical coherence tomography and nerve fiber layer polarimetry are more suitable for quantitative evaluation of RNFL thickness. However, there have been no reports of in vivo quantitative measurement of RNFL in rodent retina by these methods. The radial striations of RNFL in SLO images appeared to be much stronger in Brown Norway rats than in humans. We used pigmented rats for RNFL evaluation, as visualization of RNFL by argon laser is better in pigmented than in albino rats (data not shown). This better visualization by pigmentation is probably because most of the incident light is absorbed by pigments in the retinal pigment epithelium and the choroid and then reflected light from these tissues is greatly reduced.

We then attempted to evaluate rat RNFL quantitatively by SLO. The smallest setting of the confocal aperture in the SLO used in this study was 1 mm (C1), a setting considerably larger than those in tomographic instruments. Woon et al.[11] measured the axial resolution of this SLO using a C1 confocal aperture in a human model eye and reported that the resolution was 300 μm in a 20° field of view. They used a model eye that consisted of a 16-mm lens and a micrometer mounted mirror. The pixel brightness of the SLO image of the mirror was then plotted against the axial displacement of the mirror. The full-width-at-half-maximum brightness was taken as the axial resolution. Even with this setting, the possibility of optical sectioning and in vivo three-dimensional reconstruction of the human fundus by SLO was reported.[12] Furthermore, considerably improved axial resolution can be achieved with an SLO (Rodenstock). Fitzke et al.[13] reported an optical section of 28 μm with a confocal aperture of 1 mm using a ×8 magnification system for the prototype SLO (Rodenstock).

A similar situation occurs when viewing the rat fundus by SLO. According to data of representative rat[14] and human (Gullstrand's schematic eye) eyes, the axial length of a rat eye is much shorter than that of humans (6.29 vs. 24.00 mm), and the total power of the rat eye is much greater than in humans (300.705 vs. 58.64 D). Therefore, lateral magnification of the rat fundus in SLO images should be approximately five times larger than that of the human fundus. We confirmed that SLO images of the rat fundus were approximately five times larger than images of the human fundus, with the size of the rat and human optic discs (~300 vs. 1500 μm in diameter) being similar in SLO images with the same size field of view. Given that axial magnification is determined by the square of the lateral magnification, the axial magnification of the SLO images of a rat fundus should therefore have been approximately 25 times larger than those of humans in a field of view of the same size. Therefore, when taking SLO images in a 40° field of view, as used in this study, the axial magnification of a rat fundus will be 6.25 times larger than human SLO images in a 20° field of view with the axial resolution of 300 μm.[11] Accordingly, the axial resolution of the rat SLO images would have been approximately 50 μm in this study. Given that the thickness of human and rat retina are similar (typically 250 vs. 170 μm[14]), optical sectioning of a rat fundus by an SLO (Rodenstock) should be superior to that achieved in humans.

As for the 1-D step of the ametropic corrector to evaluate RNFL thickness in this study, adding 1 D to the ametropic correction moves the plane of focus approximately 0.3 mm in the direction of the vitreous in the human eye, because adding 1 D to the total power of the human eye makes the posterior focal length approximately 0.3 mm shorter in Gullstrand's schematic eye. In contrast, the posterior focal length in a rat eye[14] is calculated to be approximately 10 μm shorter when adding 1 D to the total power of the rat eye. Thus, a 1-D step in the ametropic correction moves the focal plane approximately 10 μm, a step that is not too wide for measuring RNFL thickness (≤25 μm) with an axial resolution of approximately 50 μm.

In agreement with the theoretical consideration of the ability of the SLO for optical sectioning of a rat fundus, the focus measurement of rat RNFL (ΔF) using this technique was performed successfully with good intra- and interobserver reproducibility using a 1-mm confocal aperture.

In the next step, we compared the ΔF and the actual RNFL thickness in histologic sections to verify that ΔF is a reliable indicator of RNFL thickness. Although RNFL thickness may vary at different distances from the optic disc, we consistently measured the RNFL thickness at a location approximately 500 μm temporal from the center of the optic disc. At this location, the visibility of radial striations of RNFL in SLO images was suitable for determination of the ΔF value and also the RNFL was thick enough for measuring the changes in retinal sections.

Given a nominal 1-D step of the ametropic corrector corresponding to approximately 10-μm movement of the focal plane and the axial resolution of approximately 50 μm (full-width-at-half-maximum brightness) in SLO images of rat fundus, the ΔF of approximately 7 D for the 25-μm thickness of normal rat RNFL is reasonable. In contrast, ΔF was approximately 1 D for <5 μm of RNFL thickness in the retina 4 weeks after the optic nerve crush, although it should have been ≥5 D, theoretically. This discrepancy may be explained as follows. The half-maximum brightness of the normal rat RNFL reflex in SLO images may be similar to the threshold of seeing the reflex. However, for thinner RNFL, the visibility became lower, and then stricter focusing (i.e., smaller ΔF values) may have been needed to see the reflex.

The significant positive relationship between ΔF and the histologically determined RNFL thickness indicates that ΔF is a reliable indicator of actual RNFL thickness and, thus, quantitative analysis of rat RNFL can be performed by SLO.

The RNFL thickness was unchanged until the first week after the optic nerve crush in SLO images and retinal sections. Furthermore, we did not notice any qualitative changes of the RNFL reflex in either SLO images or intraretinal axon bundles in histologic sections between baseline and 1 week after the crush. As for the loss of retinal ganglion cell bodies after the optic nerve crush or axotomy, the time course and magnitude of cell death depends on the severity of the injury[15,16] and the distance of the injury site from the ganglion cell bodies.[17] When the optic nerve is damaged intraorbitally, ganglion cell death starts several days after injury,[18] reaches 30% to 50% 1 week after,[19–21] and progresses further thereafter. In this study, as an index of ganglion cell loss, we counted the number of cells in the ganglion cell layer in the retinal sections used for measuring RNFL thickness and found that the decrease in cell counts was significant 1 week after the crush. Thus, the result of this study suggests that loss of cell bodies may precede the loss of intraretinal axons of retinal ganglion cells after the optic nerve crush. The implication of dissociation between the time course of changes in intraretinal axons and cell bodies is currently unknown. Given that retinal ganglion cells of the adult rat die through apoptosis when axotomized,[22] the clearance processes for apoptotic cell bodies may differ from those for intraretinal axons. Further studies are needed to examine this hypothesis.

In conclusion, SLO is a useful and valuable tool for in vivo imaging and quantification of rat RNFL. Evaluation of rat RNFL by SLO will be informative not only in optic nerve crush models but also in other models of optic nerve damage for studying the pathology of optic neuropathy including glaucoma and for developing new therapies.

References

1. Blumenthal EZ, Weinreb RN. Assessment of the retinal nerve fiber layer in clinical trials of glaucoma neuroprotection. *Surv Ophthalmol.* 2001;45:S305-S312.
2. Miglior S, Rossetti L, Brigatti L, Bujtar E, Orzalesi N. Reproducibility of retinal nerve fiber layer evaluation by dynamics scanning laser ophthalmoscopy. *Am J Ophthalmol.* 1994;118:16-23.
3. Nishiwaki H, Ogura Y, Kimura H, Kiryu J, Honda Y Quantitative evaluation of leukocyte dynamics in retinal microcirculation. *Invest Ophthalmol Vis Sci.* 1995;36:123-130.
4. Goldblum D, Mittag T Prospects for relevant glaucoma models with retinal ganglion cell damage in the rodent eye. *Vision Res.* 2002;42:471-478.
5. Allcutt D, Berry M, Sievers J. A quantitative comparison of the reactions of retinal ganglion cells to optic nerve crush in neonatal and adult mice. *Brain Res.* 1984;318:219-230.
6. Villegas-Perez MP, Vidal-Sanz M, Bray GM, Aguayo AJ. Influences of peripheral nerve grafts on the survival and regrowth of axotomized retinal ganglion cells in adult rats. *J Neurosci.* 1988;8:265-280.
7 Chauhan BC, Pan J, Archibald ML, LeVatte TL, Kelly ME, Tremblay F. Effect of intraocular pressure on optic disc topography, electroretinography, and axonal loss in a chronic pressure-induced rat model of optic nerve damage. *Invest Ophthalmol Vis Sci.* 2002; 43:2969-2976.
8. Mabuchi F, Aihara M, Mackey MR, Lindsey JD, Weinreb RN. Optic nerve damage in experimental mouse ocular hypertension. *Invest Ophthalmol Vis Sci.* 2003;44:4321-4330.
9. Allcutt D, Berry M, Sievers J. A qualitative comparison of the reactions of retinal ganglion cell axons to optic nerve crush in neonatal and adult mice. *Brain Res.* 1984;318:231-240.
10. Sugiyama K, Gu ZB, Kawase C, Yamamoto T, Kitazawa Y Optic nerve and peripapillary choroidal microvasculature of the rat eye. *Invest Ophthalmol Vis Sci.* 1999;40:3084-3090.
11. Woon WH, Fitzke FW, Bird AC, Marshall J. Confocal imaging of the fundus using a scanning laser ophthalmoscope. *Br J Ophthalmol.* 1992;76:470-474.
12. Fitzke FW, Masters BR. Three-dimensional visualization of confocal sections of *in vivo* human fundus and optic nerve. *Curr Eye Res.* 1993;12:1015-1018.
13. Fitzke FW, Woon H, Timberlake G, Robinson L, Marshall J, Bird AC. Optical modifications to a scanning laser ophthalmoscope for high magnification, narrow optical section imaging. *Lasers Light Ophthalmol.* 1991;4:7-14.
14. Hughes A. A schematic eye for the rat. *Vision Res.* 1979;19:569-588.
15. Berkelaar M, Clarke DB, Wang YC, Bray GM, Aguayo AJ. Axotomy results in delayed death and apoptosis of retinal ganglion cells in adult rats. *J Neurosci.* 1994;14:4368-4374.
16. Gellrich NC, Schimming R, Zerfowski M, Eysel UT. Quantification of histological changes after calibrated crush of the intraorbital optic nerve in rats. *Br J Ophthalmol.* 2002;86:233-237
17 Villegas-Perez MP, Vidal-Sanz M, Rasminsky M, Bray GM, Aguayo AJ. Rapid and protracted phases of retinal ganglion cell loss follow axotomy in the optic nerve of adult rats. *J Neurobiol.* 1993;24:23-36.
18. Levkovitch-Verbin H, Quigley HA, Martin KRG, Zack DJ, Pease ME, Valenta DF. A model to study differences between primary and secondary degeneration of retinal ganglion cells in rats by partial optic nerve transaction. *Invest Ophthalmol Vis Sci.* 2003;44: 3388-3393.
19. Barron KD, Dentinger MP, Krohel G, Easton SK, Mankes R. Qualitative and quantitative ultrastructural observations on retinal ganglion cell layer of rat after intraorbital optic nerve crush. *J Neurocytol.* 1986;15:345-362.
20. Mansour-Robaey S, Clarke DB, Wang YC, Bray GM, Aguayo AJ. Effects of ocular injury and administration of brain-derived neurotrophic factor on survival and regrowth of axotomized retinal ganglion cells. *Proc Natl Acad Sci USA.* 1994;91:1632-1636.
21. Selles-Navarro I, Ellesam B, Fajardo R. Retinal ganglion cell and nonneural cell responses to a microcrush lesion of adult rat optic nerve. *Exp Neurol.* 2001;167:282-289.
22. Garcia-Valenzuela E, Gorczyca W, Darzynkiewicz Z, Sharma SC. Apoptosis in adult retinal ganglion cells after axotomy. *J Neurobiol.* 1994;25:431-438.

In Vivo Imaging and Counting of Rat Retinal Ganglion Cells Using a Scanning Laser Ophthalmoscope

Tomomi Higashide, Ichiro Kawaguchi, Shinji Ohkubo, Hisashi Takeda, and Kazuhisa Sugiyama

Purpose. To determine whether a scanning laser ophthalmoscope (SLO) is useful for in vivo imaging and counting of rat retinal ganglion cells (RGCs).

Methods. RGCs of Brown Norway rats were retrogradely labeled bilaterally with the fluorescent dye 4-(4-(dihexadecylamino)styryl)-*N*-methylpyridinium iodine (DiA). The unilateral optic nerve was crushed intraorbitally with a clip. RGCs were imaged in vivo with an SLO with an argon blue laser (488 nm) and optical filter sets for fluorescein angiography, before and 1, 2, and 4 weeks after the crush. Fluorescent cells were also counted in retinal flatmounts at baseline and 1, 2, and 4 weeks after the crush. An image overlay analysis was performed to check cell positions in the SLO images over time. Lectin histochemical analysis was performed to determine the relationship of microglia to the newly emerged DiA fluorescence detected by image overlay analysis after the optic nerve crush.

Results. Fluorescent RGCs were visible in vivo with an SLO. RGC survival decreased gradually after the crush. In the retina after the optic nerve crush, newly emerged DiA fluorescence detected by image overlay analysis corresponded to fluorescent cells morphologically different from RGCs in the retinal flatmount and was colocalized mostly with lectin-stained microglial processes. RGC counts by SLO were comparable to those in retinal flatmounts.

Conclusions. The SLO is useful for in vivo imaging of rat RGCs and therefore may be a valuable tool for monitoring RGC changes over time in various rat models of RGC damage. (*Invest Ophthalmol Vis Sci.* 2006;47:2943–2950) DOI:10.1167/iovs.05-0708

Ocular hypertension, ischemia-reperfusion, and optic nerve crush rodent models have helped elucidate the pathophysiology of glaucoma and other optic neuropathies.[1] In these models, the number of retinal ganglion cells (RGCs) is usually counted in retinal flatmounts that are prepared after labeling of RGCs, then the changes of RGCs are evaluated by comparing the equivalent retinal positions in experimental and control eyes.[2–4] However, inconsistency of staining efficacy or inherent variability of RGC density[5] prevents detection of small differences in RGC survival between experimental and control eyes.

Examination of RGC changes in vivo over time may overcome this drawback. Only a few papers have reported successful imaging of rat RGCs in vivo with a confocal laser scanning microscope,[6] a fluorescence microscope,[7] or conventional infrared fundus photography.[8] Recently, in vivo imaging of RGC apoptosis using a confocal laser scanning microscope has been reported.[9] However, imaging techniques using a confocal laser scanning microscope or a fluorescence microscope have not been widely adopted because of the limited availability of the equipment and the necessary special modifications of the microscope. Counts of RGCs made with infrared fundus photography have not been published. Therefore, a new methodology for in vivo imaging of RGCs is needed.

The scanning laser ophthalmoscope (SLO) is widely used in fluorescein and indocyanine green angiography to examine human retinal diseases. Furthermore, the SLO has been reported to be useful for evaluation of the retinal nerve fiber layer and the optic disc of human glaucomatous eyes.[10,11] The SLO can also be used for imaging rat retinas to study retinal microcirculation.[12] In this study, we wanted to determine whether the SLO is useful for in vivo imaging and counting of rat RGCs by using the optic nerve crush model.

Methods

Animals

Male Brown Norway rats, 12 weeks of age and weighing 200 to 250 g, were used. Six rats (group 1) were used for in vivo RGC imaging by SLO over time (before and 1, 2, and 4 weeks after unilateral optic nerve crush) and to compare the SLO images and retinal flatmount images at 4 weeks after optic nerve crush. The comparison of both images in the nonsurgical eyes served as baseline data. In addition, 12 rats (group 2) were used to compare the images of SLO and retinal flatmounts at 1 and 2 weeks after optic nerve crush (6 rats for each time point). Furthermore, three rats (group 3) for each time point (baseline and 1, 2, and 4 weeks after optic nerve crush) were used for the histochemical analyses of microglia.

All animals were treated in accordance with the ARVO Statement for the Use of Animals in Ophthalmic and Vision Research. Experiments were conducted on rats anesthetized by intraperitoneal injection of pentobarbital sodium (65 mg/kg).

Retrograde Fluorescent Staining of RGCs

Retrograde staining of RGCs of both eyes was achieved by injecting a fluorescent dye into the superior colliculus bilaterally. Rats were placed in a stereotactic apparatus (Narishige Co. Ltd., Tokyo, Japan), and the skin of the skull was incised. The brain surface was exposed by perforating the parietal bone with a dental drill to facilitate dye injection. A fluorescent dye, 4-(4-(dihexadecylamino)styryl)-*N*-methylpyridinium iodine (DiA; Invitrogen, Eugene, OR), was dissolved in dimethylformamide (Sigma-Aldrich, St. Louis, MO) at a concentration of 10 μg/mL. The dye solution (2.0 μL) was injected at a point 5.5 mm caudal to the bregma and 1.5 mm lateral to the midline on both sides to a depth of 4.5 mm from the surface of the skull, in accordance with the results of preliminary experiments to identify the position of the superior colliculus.

From the Department of Ophthalmology, Kanazawa University Graduate School of Medical Science, Kanazawa, Japan.

Supported by a Grant-in-Aid for Scientific Research from the Ministry of Education, Science, and Culture, Japan.

Submitted for publication June 7, 2005; revised October 27, 2005, and February 23, 2006; accepted May 15, 2006.

Disclosure: **T. Higashide**, None; **I. Kawaguchi**, None; **S. Ohkubo**, None; **H. Takeda**, None; **K. Sugiyama**, None

The publication costs of this article were defrayed in part by page charge payment. This article must therefore be marked "*advertisement*" in accordance with 18 U.S.C. §1734 solely to indicate this fact.

Corresponding author: Tomomi Higashide, Department of Ophthalmology, Kanazawa University Graduate School of Medical Science, 13-1 Takara-machi, Kanazawa, Ishikawa 9208641, Japan; eyetomo@kenroku.kanazawa-u.ac.jp.

In Vivo Imaging of RGCs with the SLO

The eyes were dilated with 0.5% tropicamide and 0.5% phenylephrine hydrochloride eye drops (Santen Pharmaceuticals, Osaka, Japan). To preserve corneal clarity throughout the experiment, we placed a custom-made contact lens with a radius of curvature of 2.75 mm and a diameter of 5.0 mm (Kyoto Contact Lens, Kyoto, Japan) on the cornea after topical anesthesia with 0.4% oxybuprocaine hydrochloride eye drops (Santen Pharmaceuticals). A rat was placed on a heating pad (Deltaphase Isothermal Pad; Braintree Scientific, Inc., Braintree, MA), and its head was gently held manually to keep the eye in position for viewing the fundus with an SLO (SLO 101; Rodenstock Instruments, Munich, Germany). Under illumination with an argon blue laser (488 nm), we focused on the retinal surface by changing the refractive values in the SLO setting, visualizing fluorescent RGCs through the optical filter sets for fluorescein angiography. Dynamic fundus images with a field angle of 40° were recorded in the center of the fundus and also in the midperipheral area. The SLO images were digitized by an analog-to-digital video converter (Canopus ADVC-300; Canopus Co., Ltd., Kobe, Japan) and saved as DV-AVI files on a computer (VAIO VGC-RA50S; Sony Corp., Tokyo, Japan), running commercial computer software (DV GatePlus; Sony Corp.). In vivo images of RGCs were obtained before and 1, 2, and 4 weeks after optic nerve crush.

Intraorbital Optic Nerve Crush

Intraorbital optic nerve crush was performed 2 months after the retrograde staining of RGCs because we observed a gradual increase in the intensity and the area of RGC staining for up to 2 months after dye injection (data not shown). The conjunctiva of the right eye was incised in the superotemporal quadrant to expose the optic nerve by careful blunt dissection under an operating microscope. The optic nerve was crushed 2 mm behind the globe for 30 seconds with a 60-g clip (Micro Vascular Clip; Roboz Surgical Instrument Co., Gaithersburg, MD). Special care was taken not to damage the blood supply to the eye. The fundus was monitored by indirect ophthalmoscopy, and immediate recovery of retinal blood supply was observed in each eye after removal of the clip. The left eye had no operation.

Retinal Flatmounts

In group 1 rats, both eyes were subjected to retinal flatmount preparation 4 weeks after the optic nerve crush. In group 2 and 3 rats, the retinal flatmounts were prepared from the right eye.

Immediately after in vivo imaging of RGCs, the eyes were enucleated after administration of an overdose of anesthesia by an intraperitoneal injection of pentobarbital sodium. The anterior segments were removed, and the resultant posterior eye cups were fixed in 4% paraformaldehyde and 0.1 M phosphate-buffered saline (PBS) for 1 hour at room temperature. After six radial cuts were made in the periphery of the eye cup, the retina was carefully separated from the retinal pigment epithelium. A small marking cut was placed in the peripheral corner of the superior retinal portion for the correct identification of the retinal orientation. The retina was then flatmounted on a glass slide, covered with an antifade mounting solution (Vectashield; Vector Laboratories, Burlingame, CA) and glass coverslip, and kept in the dark at 4°C until microscopic observation.

RGCs in the retinal flatmounts were examined with a fluorescence microscope (Nikon Eclipse TE300; Nikon Corp., Kanagawa, Japan) equipped with a filter set (excitation filter 450 to 490 nm; barrier filter 520 nm; B-2A; Nikon) and 10× objective. RGC images were recorded as JPEG files with a digital cooled charge-coupled device camera (DS-5Mc-L1; Nikon) and were stored on a computer (Dimension 8300; Dell Inc., Round Rock, TX).

Image Analysis for Cell Counting

A retinal area 0.5 to 1.5 mm from the center of the optic disc, where cells were intensely stained and were well focused in SLO images throughout the experimental period, was selected for each eye. Still images of the selected retinal area were created from the DV-AVI files of dynamic SLO images by using video-editing software (Premiere 6.5; Adobe Systems Inc., Mountain View, CA). The identical retinal area of the same eye was determined in SLO images obtained at different times and also in the flatmount images by using image-editing software (Photoshop, ver. 6.0; Adobe Systems Inc.). The number of labeled cells in the selected area of each image was counted manually in a masked fashion by the same investigator. Small spots of punctate fluorescence observed in the flatmounted images after the optic nerve crush were not included in the cell count because they represented cell debris of dead RGCs (see Fig. 2J, arrows).[13] When counting RGCs only, we applied the morphologic criteria for discriminating non-RGC cells from RGCs.[13,14] Cells with irregular shape, intense DiA staining, and smaller or larger size than typical RGCs (see Fig. 5D) were considered to be non-RGC cells such as microglia (see Fig. 5, arrows in 5H, 5L, 5P). The size of the retinal area for RGC counting was measured in the flatmount images using image-analysis software (Image-Pro Express 4.0; Media Cybernetics, Inc., Silver Spring, MD), and the density of labeled cells in each image was calculated.

Image Overlay Analysis

To distinguish RGCs from other types of cells, which presumably were microglial cells that became fluorescent by phagocytosis of cell debris of RGCs after optic nerve crush, an image overlay analysis was performed. The cell positions in the SLO images taken after optic nerve crush were compared with those at baseline in the analysis. Because RGCs are not mobile and are stably labeled by retrograde transport of DiA 2 months after dye injection, fluorescent cells that have emerged in a location where no fluorescence was observed before should be other types of cells. With the image analysis software (Photoshop; Adobe Systems, Inc.), the SLO images recorded before optic nerve crush had their brightness inverted and were overlaid as a 50% opaque layer onto the SLO images of the same retinal area taken after axonal injury. Theoretically, if the precrush image were identical with the postcrush image, the composite image, which is produced by the overlay with perfect alignment of the two images, would become homogeneously gray. Slight misalignment of identical spots in the two images produces a shadowing effect around the spots. In contrast, fluorescent spots that disappeared or emerged after the crush should appear as black or white spots in the composite images. The image

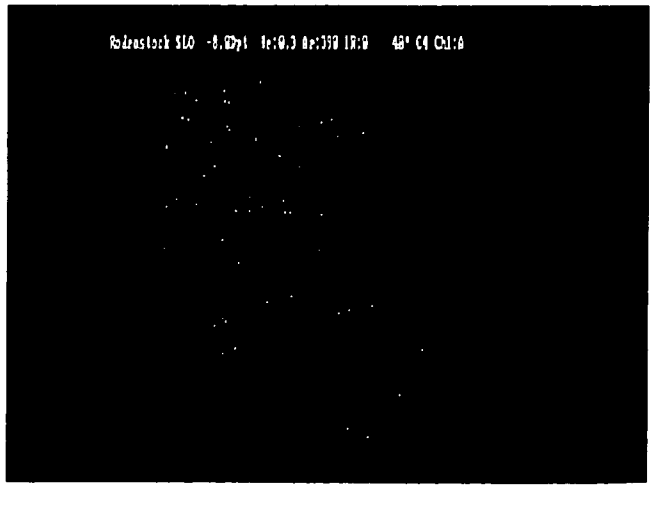

FIGURE 1. Representative SLO image of normal rat retina showing retinal ganglion cells (RGCs) retrogradely labeled with DiA. SLO imaging was performed with an argon blue laser (488 nm) and optical filter sets for fluorescein angiography. Labeled RGCs are visible as *white* spots.

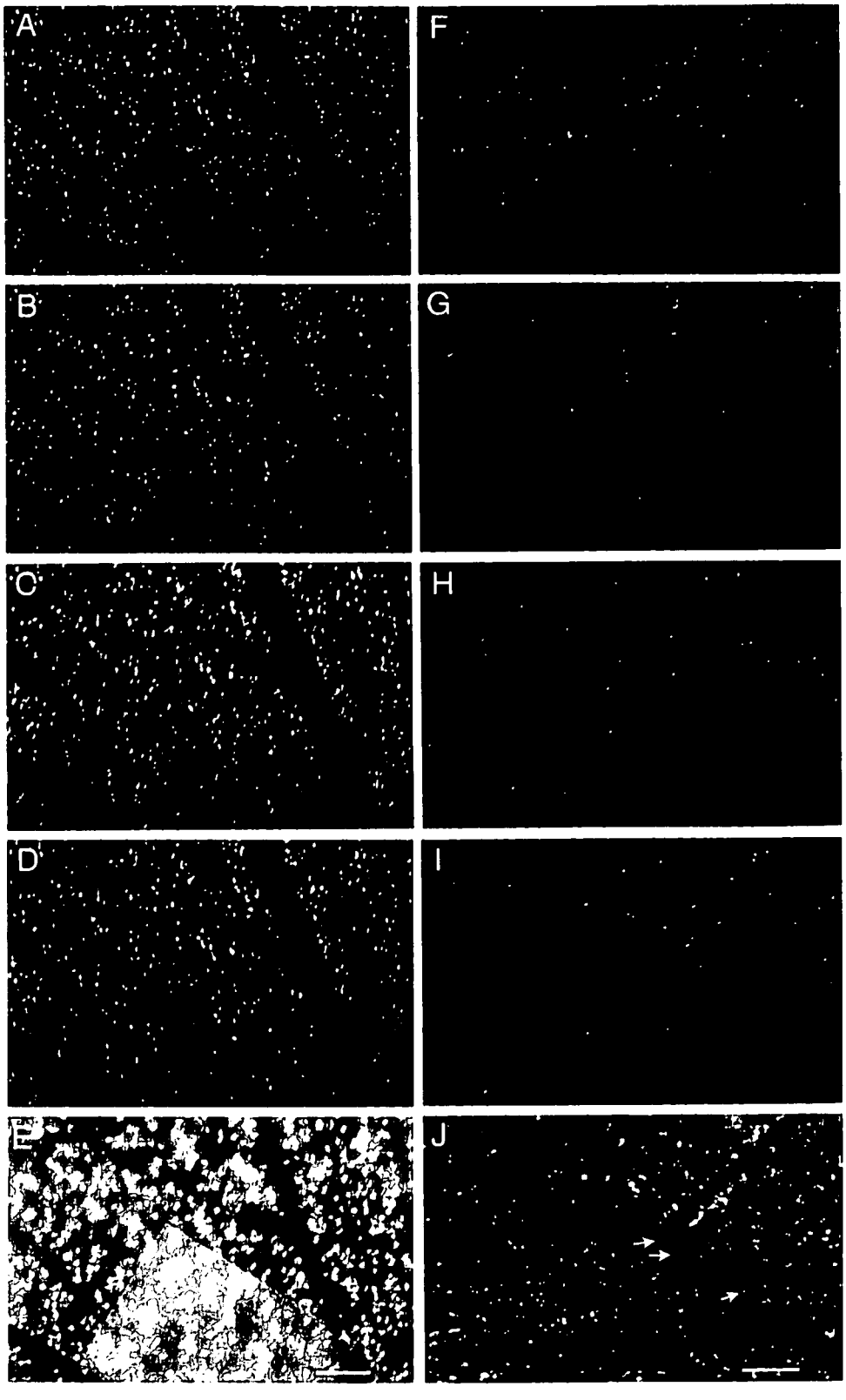

FIGURE 2. Representative photographs showing the changes of DiA-labeled cells in the same retinal area of control (A–E) and experimental (F–J) eyes. (A–D, F–I) SLO images; (E, J) flatmount images. The optic nerve of the right eye was crushed intraorbitally with a clip. The left eye served as the untreated control. SLO imaging of the same retinal area of control and experimental eyes was performed before (A, F) and at 1 (B, G), 2 (C, H), and 4 (D, I) weeks after axonal injury. Retinal flatmounts of control (E) and experimental (J) eyes were prepared after the SLO imaging at postcrush week 4, and the same retinal areas of SLO images were examined by fluorescence microscopy. *Arrows*: small spots of punctate fluorescence representing cell debris of dead RGCs. Scale bar, 100 μm.

overlay system was used in the rats in group 1 (for control and 4 weeks after the crush) and group 2 (for 1 and 2 weeks after the crush). The composite SLO images were compared with the identical retinal area in the flatmounts. RGC counts in SLO images were determined by subtracting the number of newly-emerged fluorescent cells from total cell counts.

Histochemical Analysis of Microglia

For the group 3 rats, SLO imaging of RGCs was performed at baseline and at the time when the retinal flatmounts were to be prepared. After obtaining images of DiA-labeled RGCs with an SLO in vivo and with a fluorescence microscope (Axioplan 2; Carl Zeiss GmbH, Jena, Ger-

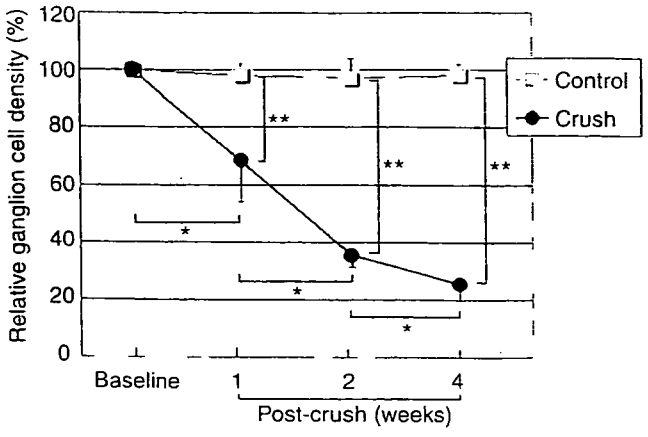

FIGURE 3. The DiA-labeled cell density after optic nerve crush determined by SLO. The relative density of labeled cells in selected retinal areas of an SLO image at each time point was determined in each eye, with labeled cell density of the SLO image taken at baseline being 100%, and the results were averaged. Data are presented as the mean ± SD (n = 6 each). *$P < 0.01$ (Wilcoxon signed rank test), **$P < 0.01$ (Wilcoxon rank sum test).

many) with a filter set (equivalent to B-2A; Nikon) in the flatmounted retina, we performed histochemical staining of microglia[15] in the flatmounted retina. The glass coverslip covering the retinal flatmounts was carefully removed. The retina was floated in PBS, flatmounted on a nylon membrane (Hybond-N+; GE Healthcare, Piscataway, NJ), and blocked with 0.5% bovine serum albumin in PBS and 1.0% Triton X-100 at room temperature for 1 hour. The retina was then incubated with 20 μg/mL of biotin-conjugated isolectin B4 from *Griffonia simplicifolia* (Sigma-Aldrich, Inc.) in PBS with 0.5% bovine serum albumin and 0.5% Triton X-100 at 4°C overnight. After it was washed in PBS, the retina was treated with 10 μg/mL of Alexa Fluor 350-conjugated avidin (NeutrAvidin; Invitrogen) in PBS with 0.5% bovine serum albumin and 0.1% Triton X-100 at room temperature for 2 hours. The retina was then washed in PBS, carefully peeled from the nylon membrane, flatmounted on a glass slide, and covered with antifade medium (Vectashield; Vector Laboratories) and a glass coverslip. Fluorescence of Alexa Fluor 350 labeling was examined using a fluorescence microscope (Axioplan; Carl Zeiss GmbH) with an appropriate filter set for the dye. The cell density of the microglia was measured at four retinal locations (500 × 500 μm^2 each, 1–1.5 mm from the center of the optic disc) per eye and averaged.

Statistical Analysis

The relative density of labeled cells in the selected retinal area of an SLO image at each time point or of the flatmount image was determined for each eye with the labeled cell density of the SLO image taken before the optic nerve crush being 100%. Differences in cell densities were statistically analyzed by the Wilcoxon rank sum test for comparison between control and crushed eyes and by the Wilcoxon signed rank test for comparison of SLO images taken at different time points and of cell densities between SLO and flatmount images. For the comparison of image overlay analysis and retinal flatmounts, differences in RGC counts by SLO and those in retinal flatmounts were also examined by the Wilcoxon signed rank test. One-way ANOVA tests and post hoc tests were used to assess changes of microglial cell densities caused by optic nerve crush. $P < 0.05$ was considered statistically significant. Data are expressed as the mean ± SD.

RESULTS

Fluorescent RGCs stained with DiA were visible in vivo with an SLO with argon blue laser illumination and the optical filter sets for fluorescein angiography (Fig. 1). Although the retinal area that can be viewed in a single SLO frame was limited, it was not difficult to obtain a retinal image of a desired area by aligning the direction of the rat eye manually. The entire image of an SLO frame could not be focused well simultaneously. However, at least 0.1 mm^2 of retinal area could be focused well simultaneously in an SLO frame. The retinal area used for cell counting in retinas of group 1 in the flatmount preparation was 0.30 ± 0.15 mm^2 (n = 12). The baseline labeled cell density (cell number/retinal area) of the selected retinal areas in both eyes of group 1 rats was 1967 ± 377 cells/mm^2 (n = 12).

After the optic nerve crush, a decrease in fluorescent cells in selected retinal areas of the SLO image was significant at 1 week and progressed at 2 and 4 weeks (Figs. 2, 3). The number of labeled cells in the untreated control eyes remained stable during the experimental period (Figs. 2, 3). To evaluate the validity of cell counts in the SLO images, the number of labeled cells was also determined in retinal flatmounts. The relative density of DiA-labeled cells in SLO images (with that in retinal flatmounts being 100%) was 101.5% ± 9.9%, 98.2% ± 4.8%, 91.3% ± 4.4%, and 99.6% ± 12.0% at baseline and 1, 2, and 4 weeks after optic nerve crush, respectively. Cell counts by SLO were not significantly different from those in retinal flatmounts. However, details of cell structure were less clear in SLO images than in flatmount images (Fig. 2). Furthermore, most of the punctate fluorescence, which we considered to be cell debris of dead RGCs, observed in the flatmount images of postcrush retina was not clearly visible with the SLO (Fig. 2, arrows). Thus, the resolution and sensitivity of fluorescence in SLO images were lower than those in flatmount images.

To identify non-RGC cells which became fluorescent after the optic nerve crush, we performed an image overlay analysis. The overlay composite images of control retinas showed few black or white spots, indicating that few deaths followed by phagocytosis of RGCs occurred in the control retinas during the experimental period (Fig. 4). In contrast, a significant number of black and white spots appeared in the composite images of postcrush retina. The position of white spots changed over time, reflecting the movement of the cells (Fig. 4). Thus, fluorescent spots in SLO images of postcrush retina (Fig. 2) consisted of both surviving RGCs and emerging non-RGC cells.

By comparing the composite SLO images and retinal flatmounts, we determined that the newly emerged fluorescent spots in the SLO images after the optic nerve crush corresponded with fluorescent cells with shapes and sizes different from RGCs in retinal flatmounts (Fig. 5). Therefore, we determined RGC counts in SLO images by subtracting the number of newly emerged fluorescent cells from total cells. The results were compared with RGC counts by retinal flatmounts with application of morphologic criteria[13,14] to discriminate non-RGC cells from RGCs. There were no significant differences between RGC counts by SLO and those by retinal flatmounts in control and postcrush retinas (Fig. 6).

To determine the relationship of microglia to the newly emerged DiA fluorescence after the optic nerve crush, we stained microglia in the retinal flatmounts with isolectin B4 after taking images of DiA fluorescence in SLO and retinal flatmounts. The counts of lectin-labeled microglial cell bodies were 28.3 ± 1.5, 71.3 ± 2.5, 115.3 ± 13.3, and 66.0 ± 10.4/mm^2 at baseline and 1, 2, and 4 weeks after optic nerve crush, respectively (Fig. 7). In agreement with a previous report,[16] optic nerve crush significantly increased the number of microglia, which peaked 2 weeks after the crush. Furthermore, a point-by-point comparison of the overlaid composite images of SLO and lectin-stained retinal flatmounts showed that newly emerged fluorescent spots in SLO images colocalized mostly with microglial processes and occasionally in the vicin-

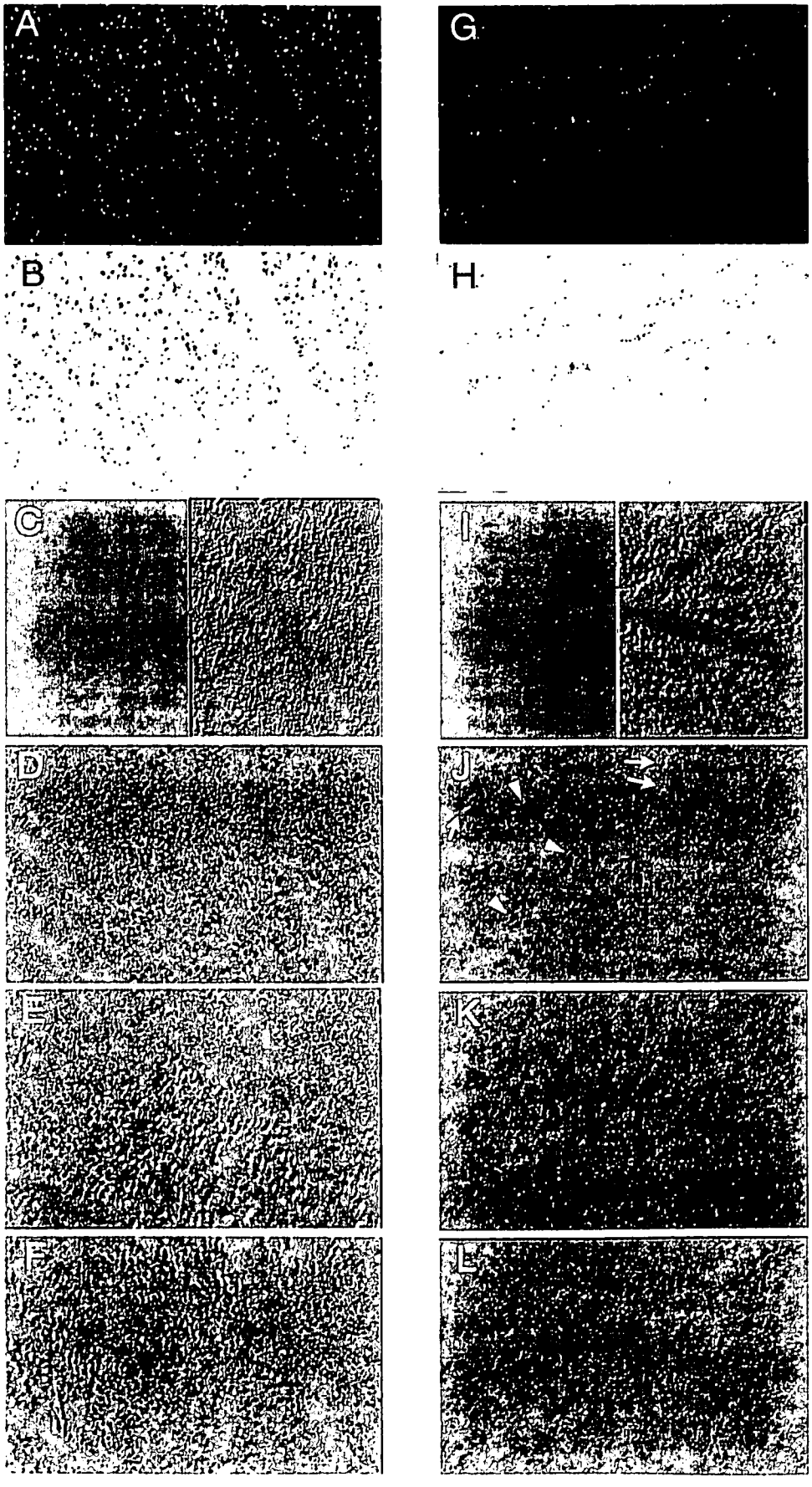

FIGURE 4. Image overlay analysis of SLO images in control (A–F) and experimental (G–L) eyes. The SLO image recorded before optic nerve crush (A, G) had its brightness inverted (B, H) and was overlaid as a 50% opaque layer, onto the SLO image of the same retinal area taken before (C, I) and 1 (D, J), 2 (E, K), and 4 (F, L) weeks after axonal injury. Although the composite image of the two identical images became homogeneously gray when they were perfectly aligned (C, I, *left* half), a shadowing effect around the spots appeared when the spots were slightly misaligned (C, I, *right* half). Fluorescent spots that disappeared or emerged in the second image should appear as *black* or *white* spots in the composite image, respectively. In control retina, few *black* and *white* spots were observed, aside from the shadowing effect (D–F). Postcrush retina showed many spots, indicating disappearing RGCs (*black*) and emerging *white* non-RGC cells (J–L). The position of *white* spots changed over time, reflecting the movement of the cells. *Arrowheads* and *arrows*: examples of *black* and *white* spots, respectively.

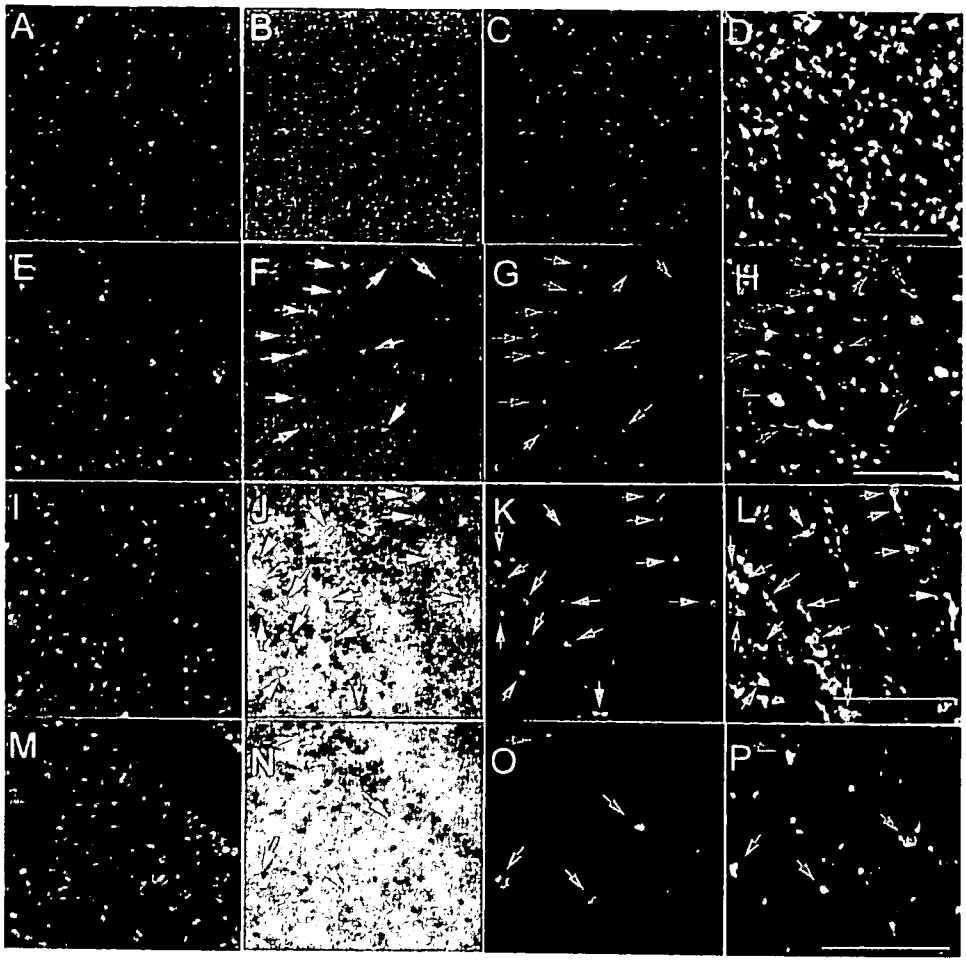

FIGURE 5. Comparison of SLO image overlay system and retinal flatmount in control (**A–D**) and postcrush (1, **E–H**; 2, **I–L**; and 4, **M–P** weeks) retinas. (**A**, **E**, **I**, **M**) baseline SLO images; (**B**, **F**, **J**, **N**) overlaid composite SLO images produced from images on both sides; (**C**, **G**, **K**, **O**) SLO images taken immediately before preparation of retinal flatmounts; (**D**, **H**, **L**, **P**) identical retinal flatmount area to SLO images of C, G, K, and O, respectively. Newly emerged fluorescent spots were not present in control retinas, but were observed in postcrush retinas (**F**, **J**, **N**, *arrows*). Identical cells to those indicated are marked by *arrows* in **G**, **H**, **K**, **L**, **O**, and **P**. *Arrows* in retinal flatmounts indicate cells with sizes and shapes different from those of typical RGCs. Scale bar, 100 μm.

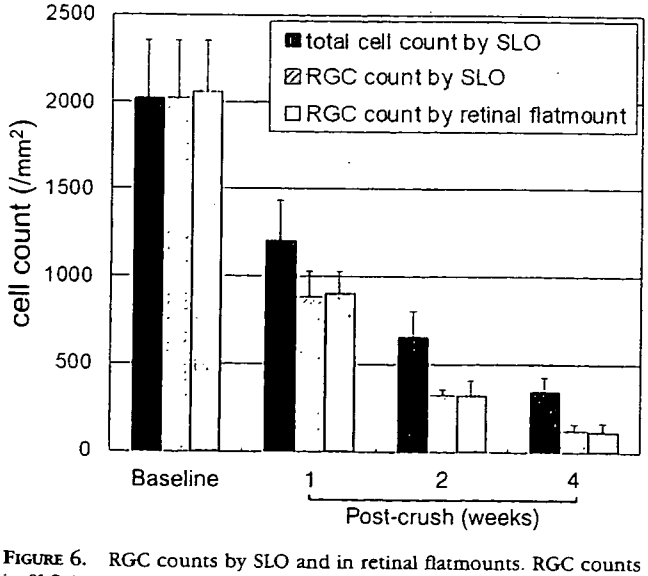

FIGURE 6. RGC counts by SLO and in retinal flatmounts. RGC counts in SLO images were determined by subtracting the number of newly emerged fluorescent cells from total cell counts. Morphologic criteria for discriminating non-RGC cells from RGCs were applied to RGC counting in retinal flatmounts. RGC counts by SLO are not significantly different from those in retinal flatmounts. Data are presented as the mean ± SD (n = 6 each).

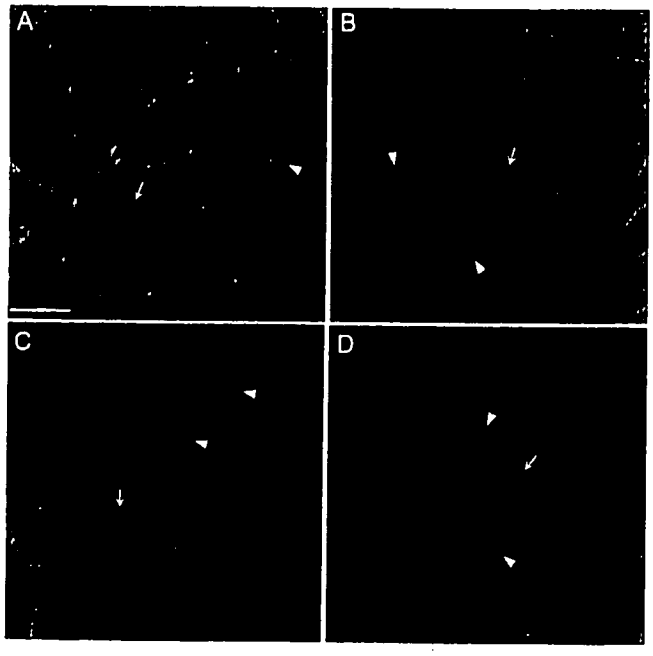

FIGURE 7. Lectin-stained microglia in retinal flatmounts. Representative photographs of retinal flatmounts at baseline (**A**), and 1 (**B**), 2 (**C**), and 4 (**D**) weeks after optic nerve crush. Lectin-stained cell bodies (*arrows*) and processes (*arrowheads*) of microglia increased after optic nerve injury, which peaked 2 weeks after the crush. Retinal vessels are also stained by lectin. Scale bar, 100 μm.

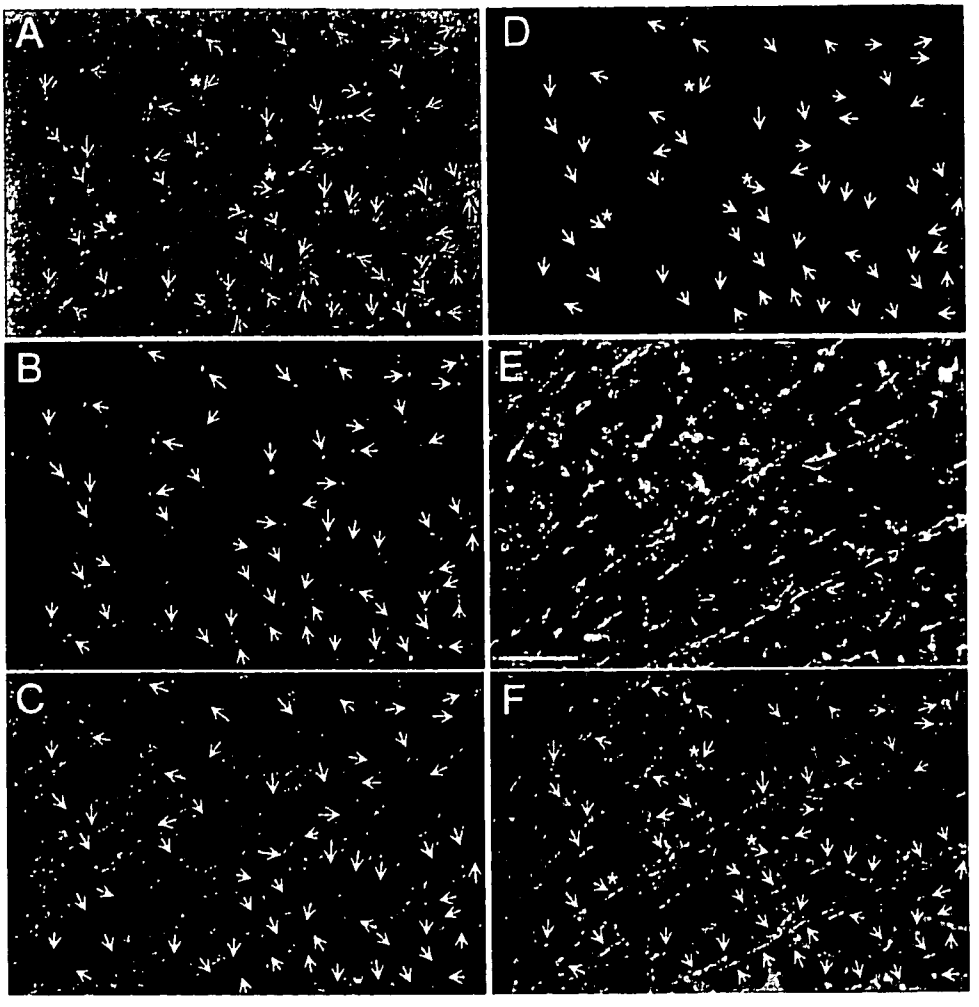

FIGURE 8. Example of point-by-point comparison of newly emerged fluorescent spots in SLO images and lectin-stained microglia. (**A**) Newly emerged fluorescent spots were marked by *arrows* in the overlaid composite images of baseline (**C**) and 2 weeks after optic nerve crush (**B**). (**B**, **C**, *arrows*) Identical positions to those in (**A**). The same retinal positions highlighted by *arrows* in (**B**) were carefully marked on the retinal flatmount showing DiA fluorescence 2 weeks after the crush (**E**). Identical *arrow* positions in (**E**) can be located on the lectin-stained flatmount (**D**) by making a superimposed image (**F**) of (**D**) and (**E**). Blood vessels showing lectin binding facilitate the correct positioning of the two images. By comparing *arrows* in (**A**) and (**D**), newly emerged fluorescent spots in SLO images appear to colocalize mostly with microglial processes and occasionally within the vicinity of microglial cell bodies (*). Scale bar, 100 μm.

ity of microglial cell bodies (Fig. 8). The colocalization was observed 1, 2, and 4 weeks after optic nerve crush.

DISCUSSION

Imaging of living RGCs in vivo has definite advantages for counting RGCs over conventional microscopic observation in flatmount retina preparations. In the histologic assessment, the number of RGCs in the selected sampling areas (usually <10% of the entire retina) are averaged and compared between eyes of the same or different rats. Accordingly, the number of RGCs and their distribution in the retina are assumed to be the same in the right and left eyes and in different animals. Also, consistent labeling of RGCs is another essential premise that can never be proven exactly until the total number of RGCs is counted. However, Danias et al.[5] pointed out the inherent problem of RGC counting by a sampling method in retinal flatmounts. They reported considerable variability of RGC density in different eyes of Wistar rats by counting RGCs in the entire retina and estimated that nearly 20 animals are necessary for the detection of a 20% difference between control and experimental eyes when 25% of the retinal area is used for cell counting. However, in vivo imaging allows repeated counting of RGCs in the same retinal area without being affected by the variability of staining and density of RGCs in different retinas. Therefore, if the same sampling procedure were used to detect the difference between pre- and posttreatment status, in vivo imaging would need fewer animals than histologic methods.

In this study, we used an SLO and repeatedly imaged RGCs successfully in vivo. Visualization of fluorescent cells in vivo with an SLO was reported by Nishiwaki et al.[12] In their study, fluorescent leukocytes stained with acridine orange were counted in rat retinas in SLO images. Similarly, fluorescent RGCs were countable in SLO images in this study.

For long-term in vivo monitoring of RGCs, carbocyanines are suitable as tracers because they are nontoxic, their labeling is intense, and labeling is stable, with survival times of up to 1 year.[17,18] Among carbocyanines, DiI (1-1′-dioctadecyl-3,3,3′,3′-tetramethylindocarbocyanine perchlorate), and 4Di-10Asp (4-(4-(didecylamino)styryl)-*N*-methylpyridinium iodine) have been used for retrograde labeling of RGCs to count RGCs in retinal flatmounts.[3,4,18] Naskar et al.[4] reported the visualization of RGCs in vivo by retrograde staining with 4Di-10Asp and fluorescence microscopy. DiA is a carbocyanine dye that is widely used as an anterograde and retrograde neuronal tracer in vivo. We chose DiA as a tracer for the SLO imaging because it has an appropriate absorption and fluorescence emission property for the argon laser and optical filter sets equipped for fluorescein angiography with an SLO. However, the labeled cell density with carbocyanines is lower than that with a hydrophilic tracer (Fluorogold; Fluorochrome, Denver, CO), probably due to lower solubility of the lipophilic dyes.[19,20] The density of DiA-labeled cells in SLO images of normal rat retinas was comparable to reported densities of RGCs stained with other carbocyanines.[4,18-20] Furthermore, the extent of decrease in of labeled cells after axonal injury agreed with that in previous

reports,[21,22] and the number of labeled cells in control eyes was constant during the experimental period. Thus, DiA is a suitable tracer for in vivo imaging of RGCs with an SLO.

We encountered several problems in SLO imaging of RGCs. First, the whole area of a single SLO frame (40°) could not be focused well simultaneously because of the image distortion by the contact lens and the spherical property of the eye. Although the minimum well-focused area was larger than the area for RGC counting in retinal flatmounts in other studies,[2,4,19,23] modification of a contact lens to enlarge the well-focused area would improve the quality of SLO images and save recording and analysis time. Second, peripheral fundus areas were difficult to image with an SLO. We selected a sampling area for RGC counting 0.5 to 1.5 mm from the center of the optic disc because of the ease of focusing. However, the adult rat retina extends more than 5 mm from the center of the optic disc.[5] Therefore, an SLO is not suitable for evaluation of RGCs in the peripheral retina.

Finally, SLO image quality was not as good as that of retinal flatmounts. Although the cell density measured in SLO images was not significantly different from that determined in flatmount images, the resolution and sensitivity of fluorescence in SLO images were lower than those in flatmount images. As reported previously, cells stained by retrograde labeling are not necessarily RGCs, because other types of cells may become labeled by phagocytosis of fluorescent RGC debris.[4,15,24] Morphologic criteria were defined to distinguish RGCs from other types of cells for counting RGCs in the retinal flatmount.[13,14,25] However, the SLO images of labeled cells were not good enough for discrimination of cell types. Thus, it may be difficult to distinguish RGCs from microglial cells morphologically and to count RGCs accurately in postcrush retina in SLO images.

To discriminate RGCs from other types of cells in SLO images, we developed a new image overlay analysis. The overlaid composite images of pre- and postcrush SLO images showed that new fluorescent spots emerged and moved after the optic nerve crush. A point-by-point comparison of the SLO image overlay and the retinal flatmount in the identical retinal area revealed that the newly emerged fluorescent spots in SLO images after the crush corresponded to non-RGC cells. Therefore, it is reasonable to determine RGC counts in SLO images by subtracting the number of newly emerged fluorescent cells from total cell counts. Furthermore, similar RGC counts by SLO and retinal flatmounts indicate that the image overlay system is useful to count RGCs in SLO images.

As newly emerged fluorescent spots are thought to be microglia that became labeled by phagocytosis of dead RGCs, we compared the SLO image overlay and lectin staining of microglia in retinal flatmounts. Colocalization of most of the new fluorescent spots with microglial processes indicated that image overlay analysis can be useful to monitor the activity of microglia after optic nerve injury.

In conclusion, the SLO is useful for in vivo imaging and counting of rat RGCs and may be a valuable tool for monitoring RGC changes over time in various rat models of RGC damage. This approach will be useful for studying the pathology of optic neuropathy including glaucoma and for developing new therapies.

References

1. Goldblum D, Mittag T Prospects for relevant glaucoma models with retinal ganglion cell damage in the rodent eye. *Vision Res.* 2002;42:471-478.
2. Villegas-Perez MP, Vidal-Sanz M, Bray GM, Aguayo AJ. Influences of peripheral nerve grafts on the survival and regrowth of axotomized retinal ganglion cells in adult rats. *J Neurosci.* 1988;8:265-280.
3. Yoles E, Schwartz M. Degeneration of spared axons following partial white matter lesion: implications for optic nerve neuropathies. *Exp Neurol.* 1998;153:1-7
4. Naskar R, Wissing M, Thanos S. Detection of early neuron degeneration and accompanying microglial responses in the retina of a rat model of glaucoma. *Invest Ophthalmol Vis Sci.* 2002;43:2962-2968.
5. Danias J, Shen F, Goldblum D, et al. Cytoarchitecture of the retinal ganglion cells in the rat. *Invest Ophthalmol Vis Sci.* 2002;43:587-594.
6. Sabel BA, Engelmann R, Humphrey MF. In vivo confocal neuroimaging (ICON) of CNS neurons. *Nat Med.* 1997;3:244-247
7. Thanos S, Indorf L, Naskar R. *In vivo* FM: using conventional fluorescence microscopy to monitor retinal neuronal death *in vivo*. *Trends Neurosci.* 2002;25:441-444.
8. Paques M, Genevois O, Regnier A, et al. Axon-tracing properties of indocyanine green. *Arch Ophthalmol.* 2003;121:367-370.
9. Cordeiro MF, Guo L, Luong V, et al. Real-time imaging of single nerve cell apoptosis in retinal neurodegeneration. *Proc Natl Acad Sci USA.* 2004;101:13352-13356.
10. Miglior S, Rossetti L, Brigatti L, Bujtar E, Orzalesi N. Reproducibility of retinal nerve fiber layer evaluation by dynamic scanning laser ophthalmoscopy. *Am J Ophthalmol.* 1994;118:16-23.
11. Sugiyama K, Uchida H, Tomita G, et al. Localized wedge-shaped defects of retinal nerve fiber layer and disc hemorrhage in glaucoma. *Ophthalmology.* 1999;106:1762-1767
12. Nishiwaki H, Ogura Y, Kimura H, Kiryu J, Honda Y. Quantitative evaluation of leukocyte dynamics in retinal microcirculation. *Invest Ophthalmol Vis Sci.* 1995;36:123-130.
13. Chauhan BC, LeVatte TL, Jollimore CA, et al. Model of endothelin-1-induced chronic optic neuropathy in rat. *Invest Ophthalmol Vis Sci.* 2004;45:144-152.
14. Levkovitch-Verbin H, Quigley HA, Martin KRG, Zack DJ, Pease ME, Valenta DF. A model to study differences between primary and secondary degeneration of retinal ganglion cells in rats by partial optic nerve transaction. *Invest Ophthalmol Vis Sci.* 2003;44:3388-3393.
15. Streit WJ. An improved staining method for rat microglial cells using the lectin from Griffonia simplicifolia (GSA I-B4). *J Histochem Cytochem.* 1990;38:1683-1686.
16. Garcia-Valenzuela E, Sharma SC, Pina AL. Multilayered retinal microglial response to optic nerve transsection in rats. *Mol Vis.* 2005;11:225-231.
17. Kobbert C, Apps R, Bechmann I, Lanciego JL, Mey J, Thanos S. Current concept in neuroanatomical tracing. *Prog Neurobiol.* 2000;62:327-351.
18. Vidal-Sanz M, Villegas-Perez MP, Bray GM, Aguayo AJ. Persistent retrograde labeling of adult rat retinal ganglion cells with the carbocyanine dye dil. *Exp Neurol.* 1988;102:92-101.
19. Lafuente MP, Villegas-Perez MP, Selles-Navarro I, Mayor-Torroglosa S, Miralles de Imperial J, Vidal-Sanz M. Retinal ganglion cell death after acute retinal ischemia is an ongoing process whose severity and duration depends on the duration of the insult. *Neuroscience.* 2002;109:157-168.
20. Simon P, Thanos S. Combined methods of retrograde staining, layer-separation and viscoelastic cell stabilization to isolate retinal ganglion cells in adult rats. *J Neurosci Methods.* 1998;83:113-124.
21. Villegas-Perez MP, Vidal-Sanz M, Rasminsky M, Bray GM, Aguayo AJ. Rapid and protracted phases of retinal ganglion cell loss follow axotomy in the optic nerve of adult rats. *J Neurobiol.* 1993;24:23-36.
22. Selles-Navarro I, Ellesam B, Fajardo R. Retinal ganglion cell and nonneural cell responses to a microcrush lesion of adult rat optic nerve. *Exp Neurol.* 2001;167:282-289.
23. Klocker N, Cellerino A, Bahr M. Free radical scavenging and inhibition of nitric oxide synthase potentiates the neurotrophic effects of brain-derived neurotrophic factor on axotomized retinal ganglion cells *in vivo*. *J Neurosci.* 1998;18:1038-1046.
24. Thanos S, Kacza J, Seeger J, Mey J. Old dyes for new scopes: the phagocytosis-dependent long-term fluorescence labeling of microglial cells *in vivo*. *Trends Neurosci.* 1994;17:177-182.
25. Perry VH, Henderson Z, Linden R. Postnatal changes in retinal ganglion cell and optic axon populations in the pigmented rat. *J Comp Neurol.* 1983;219:356-368.

Association between Genetic Polymorphisms of the Prostaglandin $F_{2\alpha}$ Receptor Gene and Response to Latanoprost

Mayumi Sakurai, MSc, Tomomi Higashide, MD, PhD, Mami Takahashi, MD, Kazuhisa Sugiyama, MD, PhD

Purpose: To evaluate the relationship between polymorphisms of the prostaglandin $F_{2\alpha}$ receptor (FP receptor) gene and the effectiveness of topical latanoprost treatment in normal volunteers.

Design: Prospective nonrandomized trial.

Participants: One hundred normal volunteers were recruited into the study.

Methods: Baseline intraocular pressures (IOPs) of both eyes of 100 normal subjects were measured at 3 time points. Latanoprost (0.005%) was applied to one eye once daily for 7 days. Diurnal IOP was measured again on day 7. Response to latanoprost was evaluated by percent IOP reduction in the treated eye minus IOP fluctuations of the nontreated eye. We classified subjects by the mean diurnal percent IOP reduction (%ΔIOP) into 3 groups: low responders (%ΔIOP<10), medium responders (10≤%ΔIOP<25), and high responders (%ΔIOP≥25). Single-nucleotide polymorphisms (SNPs) in the FP receptor gene were searched, and the genotype was determined mainly by direct DNA sequencing. A promoter assay with a reporter luciferase gene was also performed.

Main Outcome Measures: Mean diurnal percent IOP reduction and genotyping of SNPs in the FP receptor gene.

Results: Ten SNPs were identified in this study. One, rs3753380, was located in the promoter region of the FP receptor gene and was significantly correlated with %ΔIOP (CC, 20.3%±1.5% [mean ± standard error]; CT + TT, 15.6%±1.2%; $P = 0.0316$). Mean diurnal percent IOP reduction was not associated with the other SNPs. When the category classified by %ΔIOP was analyzed, not only rs3753380 but also rs3766355, an SNP in intron 1, were associated with the degree of response to latanoprost. The promoter assay revealed that the C allele of rs3766355 and T allele of rs3753380 were found in constructs with lower transcriptional activity of the FP receptor gene.

Conclusions: rs3753380 and rs3766355, SNPs in the promoter and intron 1 regions of the FP receptor gene, correlate with a response to short-term latanoprost treatment in normal volunteers. The genotype of these SNPs may be an important determinant of variability in response to latanoprost. *Ophthalmology 2007;114:1039–1045*

Latanoprost, a prostaglandin $F_{2\alpha}$ analog, is widely used to lower intraocular pressure (IOP) in patients with glaucoma, although in some cases the response is unexpectedly weak. Although Aung et al[1] and Scherer[2] showed that some patients fail to respond to latanoprost treatment, it is currently unknown what is responsible for weak responses to latanoprost in different patients.

Originally received: August 4, 2006.
Accepted: March 12, 2007. Manuscript no. 2006-874.

From the Department of Ophthalmology and Visual Science, Kanazawa University Graduate School of Medical Science, Kanazawa, Japan.

Presented at: Joint Meeting of the American Academy of Ophthalmology and Asia Pacific Academy of Ophthalmology, November 2006, Las Vegas, Nevada.

Financial support: Japan Society for the Promotion of Science, Tokyo, Japan (Grant-in-Aid for Scientific Research no. 17591826).

Correspondence and reprint requests to Tomomi Higashide, MD, PhD, Department of Ophthalmology and Visual Science, Kanazawa University Graduate School of Medical Science, 13-1 Takara-machi, Kanazawa, Ishikawa 920-8641, Japan. E-mail: eyetomo@kenroku.kanazawa-u.ac.jp.

Recently, genetic polymorphisms of β-adrenergic receptors,[3–6] angiotensin-converting enzyme,[7,8] and angiotensin II type 1 receptor[8,9] were reported to affect the degree of response to certain drugs. Schwartz et al[10] reported that a single-nucleotide polymorphism (SNP) at codon 389 in the β_1-adrenergic receptor gene correlated with the degree of response to betaxolol in normal volunteers.

Because latanoprost is a highly selective agonist for the prostaglandin $F_{2\alpha}$ receptor (FP receptor),[11] the reduction of IOP by latanoprost is considered to be mainly caused by the FP receptor. The FP receptor is a 359–amino acid protein containing 7 transmembrane domains characteristic of G protein–coupled receptors.[12,13] Later cDNA analysis showed an alternative splice variant, hFPs, which has a 71–base pair (bp) insert that causes a frame shift resulting in a truncated receptor lacking the seventh transmembrane domain and intracellular carboxyl tail.[14] The FP receptor is expressed in ocular tissues, such as corneal epithelium, ciliary epithelium, the circular portion of the ciliary muscle, and the stroma and smooth muscle cells of the iris.[15–17]

ISSN 0161-6420/07/$–see front matter
doi:10.1016/j.ophtha.2007.03.025

Activation of the FP receptor leads to G_q-mediated IP_3 generation and increases in intracellular calcium[12,18,19] and triggers an increase of matrix metalloproteinases.[20–22] Up-regulation of matrix metalloproteinases degrades the extracellular matrix in the ciliary muscle[23,24] and increases uveoscleral outflow of aqueous humor, resulting in a reduction of IOP.[11,25]

It was also shown that the FP receptor is essential for early IOP response to latanoprost in the mouse eye because latanoprost had no effect on IOP in homozygous FP receptor knockout mice.[26] Therefore, it is plausible that genetic polymorphisms of the FP receptor gene may influence the degree of response to latanoprost.

In this study, we examined whether IOP reduction by latanoprost was affected by SNPs of the FP receptor gene in healthy volunteers.

Materials and Methods

Subjects

The study protocol was approved by the institutional review board of Kanazawa University School of Medical Science and followed the guidelines of the Declaration of Helsinki. We recruited 100 Japanese volunteers without a medical history of eye diseases and obtained written informed consent from each (82 male, 18 female; mean age, 24.3±0.2 years (mean ± standard error [SE]).

Intraocular Pressure Measurement and Latanoprost Treatment

The schedule of examinations was as follows. At 9 AM, 1:30 PM, and 6 PM on day 0, baseline IOPs of both eyes were measured with a Goldmann applanation tonometer (Carl Zeiss, Inc., Jena, Germany). Central corneal thickness and refraction were measured by a pachymeter (DGH-500, DGH Technology, Inc., Exton, PA) and autorefractor/keratometer (ARK-2000, Nidek Co. Ltd., Aichi, Japan), respectively. At 9 AM, 0.005% latanoprost (Xalatan, Pfizer Japan Inc., Tokyo, Japan) was applied to one eye once daily for 7 days. The other eye served as a nontreated control. Diurnal IOP was measured again on day 7. The IOP was measured by the same investigator (MT) throughout this study.

Intraocular pressure reduction at each time point was expressed according to the formula percent IOP reduction = ([*T*pre − *T*post] − [*C*pre − *C*post])/*T*pre × 100, where *T* and *C* are the IOPs of treated and control eyes, respectively, and *pre* and *post* correspond to pretreatments and posttreatments on day 0 and day 7, respectively. Intraocular pressure reduction was shown as the mean diurnal percent IOP reduction (%ΔIOP). Based on %ΔIOP, subjects were classified as low responders (%ΔIOP<10), medium responders (10≤%ΔIOP<25), or high responders (%ΔIOP≥25). Conjunctival hyperemia in the treated eye was evaluated on day 7.

Screening and Genotyping of Single-Nucleotide Polymorphisms in the Prostaglandin $F_{2\alpha}$ Receptor Gene

Single-nucleotide polymorphisms, which were located in part of the promoter and coding regions including a newly identified exon of the FP receptor gene, were screened from genomic DNA from 24 randomly selected subjects. Known SNPs in the promoter, intron 1, and 3′-untranslated regions of the gene, reported in the National Center for Biotechnology Information (NCBI) database (http://www.ncbi.nlm.nih.gov/SNP), were also selected.

Genomic DNA was extracted from peripheral leukocytes. The primers for polymerase chain reaction (PCR) amplification of the FP receptor gene were synthesized based on sequence information[12,14,27] (NCBI database, NT 026943 in Bild122). Polymerase chain reaction was performed using KOD -plus- (Toyobo Co., Ltd., Osaka, Japan) according to the manufacturer's protocol with some modifications; 500 ng of genomic DNA was used as a template, and concentrations of magnesium sulfate and primers were adjusted to 0.8 to 1 mmol/l and 0.4 μmol/l, respectively. The amplified fragments were electrophoresed on an agarose gel, recovered from the gel using SUPREC-01 (Takara Bio Inc., Shiga, Japan), and sequenced using a dye terminator cycle sequencing kit (DYEnamic ET Terminator, Amersham Biosciences Corp., Piscataway, NJ) and an automated DNA sequencer (ABI PRISM 377 DNA Sequencer, Applied Biosystems, Foster City, CA).

Genotyping of an SNP (rs3753380) in the promoter region of the FP receptor gene was performed by a method based on single-strand conformation polymorphism. After the PCR reaction, 1 μl of each PCR mixture was combined with 3 μl of loading buffer (98% formamide, 10 mmol/l ethylenediaminetetra-acetic acid, 0.3% bromophenol blue, and 0.3% xylene cyanol) and heated at 90° C for 5 minutes. The samples were electrophoresed on a nondenaturing 10% or 12% polyacrylamide gel containing 0.5 × TBE (45 mmol/l Tris, 45 mmol/l boric acid, 1 mmol/l ethylenediaminetetra-acetic acid, pH 8.5) buffer and 5% glycerol at 4° C. After electrophoresis, DNA was stained with SYBR Gold Nucleic Acid Gel Stain (Molecular Probes Inc., Eugene, OR) and visualized with an ultraviolet transilluminator.

The SNP at A938G (K313R) in exon 4 of the FP receptor gene was detected by restriction fragment length polymorphism. The amplified fragments (515 bp) were digested with Eco81I overnight at 37° C and electrophoresed on a 1.5% agarose gel. The fragments containing an A allele were not digested, whereas those containing a G allele were digested and generated 2 fragments, 228 bp and 287 bp.

Genotyping of the other SNPs was carried out by direct sequencing as described above.

Construction of the Prostaglandin $F_{2\alpha}$ Receptor–Luciferase Fusion Gene and Reporter Assay

The region from the promoter to exon 2 of the FP receptor gene was amplified from genomic DNA by PrimeSTARHS DNA polymerase (Takara Bio) using a set of primers, FPEcoRV2F (5′-GCTGATATCCTCAGAAATAACATCACACATC-3′) (−2416 to −2394) and FPHindIIIR (5′-GCGAAGCTTCTCAAAACTGT-GCAGGATTGCAG-3′) (+1632 to +1655).[27] The nucleotide position was counted from the transcription start site determined by Zaragoza et al.[27] However, the nucleotide number in this study differed from that in their data, because their DNA sequence had extra nucleotides compared with the NCBI database (NT 026943). The amplified fragment was digested with EcoRV and HindIII and inserted into the EcoRV and HindIII–digested Bluescript SK⁻. The nucleotide sequences of the cloned fragments were confirmed by DNA sequencing as above. The AccI (filled by T4 DNA polymerase)–HindIII fragment was inserted into the SmaI and HindIII–digested sites of the pGL3-Basic vector (Promega Corp., Madison, WI). Plasmids were purified by the Plasmid Midi Kit (Qiagen K. K., Tokyo, Japan) and quantified using a spectrophotometer.

HeLa cells (RIKEN Bio Resource Center, Ibaragi, Japan) were plated in each well of a 12-well culture plate (1.6×10^5 cells/well) and grown overnight in minimum essential medium containing 10% calf serum. Cells were co-transfected with 800 ng of the reporter plasmid; 16 ng of the pRL-TK vector (Promega), which served as an internal control; and 800 ng of Bluescript SK^- using Lipofectamine 2000 (Invitrogen Corp., Carlsbad, CA). After 24 hours of incubation, firefly and renilla luciferase activities were measured using the Dual-Luciferase Reporter Assay System (Promega) and a Lumat LB 9507 luminometer (Berthold Japan Co., Ltd., Tokyo, Japan).

Statistical Analyses

The relationship between %ΔIOP and genotype was analyzed using a nonparametric statistic, the Mann–Whitney *U* test. Statistical analyses between IOP or corneal thickness and genotype were performed using Student's *t* test (Stat View, version 5, Hulinks Inc., Tokyo, Japan). For analysis of categorical data (with the low responders, medium responders, and high responders classification), the chi-square test (Stat Mate III, ATMS Co., Ltd., Tokyo, Japan) was used. The Hardy–Weinberg equilibrium test and estimation of haplotype frequency based on the expectation–maximization algorithm[28] were performed using SNPAlyze (version 3.2, Dynacom Co., Ltd., Kanagawa, Japan). Student's *t* tests were performed to examine the difference between the transcriptional activities of different haplotype combinations of 4 SNPs in the FP receptor gene. A value of $P<0.05$ was considered statistically significant.

Results

Intraocular Pressure Decrease by Latanoprost Treatment

A total of 100 normal subjects (82 male, 18 female) were treated with latanoprost in one eye. The mean diurnal IOP in the treated eyes significantly decreased, from 14.0±0.2 mmHg (mean ± SE) on day 0 to 11.4±0.2 mmHg on day 7 ($P<0.0001$), and a significant IOP reduction was observed at each diurnal time point. In contrast, IOP in the control eyes was not changed (13.5±0.2 mmHg on day 0 and 13.5±0.2 mmHg on day 7). Mean diurnal percent IOP reduction in the treated eye was 18.1±1.0. Mean central corneal thickness and refraction were 557.8±3.1 μm and −4.0±0.3 diopters, respectively. Fifty-two percent of the treated eyes had conjunctival hyperemia on day 7. There was no significant correlation between %ΔIOP and central corneal thickness, refraction, or conjunctival hyperemia.

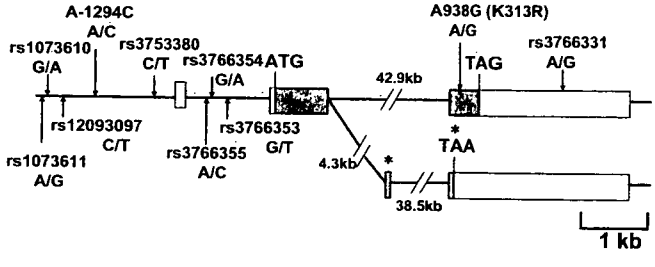

Figure 1. Structure of the prostaglandin $F_{2\alpha}$ receptor gene and the location of single-nucleotide polymorphisms (SNPs) identified in this study. The description of each SNP is available and searchable by the identification number (rsx) shown (http://www.ncbi.nih.gov/SNP). A−1294C and A938G are newly identified SNPs. Alleles (major/minor) and position of the SNPs are shown. Exons are boxed, and the coding regions are displayed with dark shading. Start and stop codons are also shown. *The coding region and stop codon produced by alternative mRNA splicing. kb = kilobase.

Table 1. Genotype of Each Single-Nucleotide Polymorphism (SNP) in the Prostaglandin $F_{2\alpha}$ Receptor Gene and Mean Diurnal Percent Intraocular Pressure Reduction

SNP Identification No.	Major Homogenotype	Minor Carrier	P*
rs1073611	17.5±1.0 (86)	21.4±2.9 (14)	0.295
rs1073610	17.5±1.0 (86)	21.4±2.9 (14)	0.295
rs12093097	17.9±1.1 (88)	19.7±2.5 (12)	0.494
A−1294C	17.6±1.0 (90)	22.3±2.9 (10)	0.173
rs3753380	20.3±1.5 (52)	15.6±1.2 (48)	0.0316
rs3766355	19.6±2.4 (25)	17.6±1.0 (75)	0.362
rs3766354	17.5±1.3 (57)	18.8±1.6 (43)	0.791
rs3766353	16.8±1.3 (46)	19.2±1.4 (54)	0.263
A938G	18.0±1.0 (96)	19.8±2.5 (4)	0.712
rs3766331	18.6±1.2 (74)	16.7±1.8 (26)	0.512

Numbers of subjects are shown in parentheses.
*Mann–Whitney *U* test.

Correlation between Mean Diurnal Percent Intraocular Pressure Reduction and Single-Nucleotide Polymorphisms

Ten SNPs in the promoter, coding, and 3′-untranslated regions of the FP receptor gene were identified and subjected to further analyses (Fig 1). Two SNPs, A−1294C in the promoter region and A938G (K313R) in exon 4, were newly identified, whereas the 8 other SNPs shown were previously reported (NCBI database). There were no polymorphisms in 19 additional SNPs that were reported previously[12,29] (NCBI database).

The relationships between %ΔIOP and SNPs of the FP receptor gene are shown in Table 1. The genotype distributions of all SNPs were in Hardy–Weinberg equilibrium ($P>0.05$), except rs1073611. Among all 10 SNPs studied, we identified a correlation between %ΔIOP by latanoprost and the genotype of one SNP, rs3753380. The %ΔIOP of subjects carrying the

Table 2. Characteristics of Subjects According to Genotypes at rs3753380

Genotypes	CC	CT + TT	P*
n (female)	52 (10)	48 (8)	0.74
Age (yrs)	24.3±0.3	24.3±0.4	1
IOP of treated eye			
Baseline (mmHg)	13.7±0.3	14.3±0.3	0.16
Day 7	10.9±0.3	12.0±0.3	0.0097
IOP of control eye			
Baseline	13.2±0.3	13.9±0.3	0.11
Day 7	13.2±0.3	13.8±0.3	0.17
Central corneal thickness of treated eye (μm)	557.2±4.8	558.5±4.0	0.84

IOP = intraocular pressure.
*t test.

Table 3. Allele and Genotype Distribution of rs3753380 and rs3766355

	Allele		Genotype			Allele		Genotype		
	C	T	CC	CT	TT	A	C	AA	AC	CC
rs3753380										
Low responders	23	15	7	9	3					
Medium responders	87	33	29	29	2					
High responders	35	7	16	3	2					
rs3766355										
Low responders						16	22	5	6	8
Medium responders						60	60	11	38	11
High responders						27	15	9	9	3

major homogenotype (CC) at rs3753380 was 20.3±1.5 (mean ± SE), whereas that of CT + TT was 15.6±1.2 (P = 0.0316). The mean diurnal IOP of the treated eyes on day 7 was significantly lower in subjects with the CC genotype (10.9±0.3 mmHg) than in those with CT + TT (12.0±0.3 mmHg) (P = 0.0097), whereas the baseline IOP level was not associated with the SNP genotype. Gender, age, and corneal thickness did not significantly differ between the CC and CT + TT genotypes (Table 2). Mean diurnal percent IOP reduction by latanoprost was not correlated with genotypes of the other SNPs.

Association of the Prostaglandin $F_{2\alpha}$ Receptor Gene Polymorphisms with Response to Latanoprost

To determine if we could predict the response to latanoprost in each patient by genetic polymorphisms of the FP receptor gene, we classified subjects by %ΔIOP into 3 groups, as described in "Materials and Methods." There were 19, 80, and 21 low, medium, and high responders, respectively. No significant differences in baseline IOPs of treated eyes, pretreatment and posttreatment IOPs of the control eyes, and corneal thickness were observed among the 3 groups.

We analyzed the relationship between each SNP of the FP receptor gene and the category of %ΔIOP. Given the allele and genotype distributions of rs3753380 and rs3766355 (Table 3), the polymorphisms in rs3753380 and rs3766355 were significantly associated with the degree of response to latanoprost (Table 4). Significant associations with response to latanoprost were found in high responders versus others (rs3753380, CC vs. CT + TT [P = 0.013; odds ratio (OR), 3.82]; rs3766355, AA vs. AC + CC [P = 0.033; OR, 2.95]) and in low responders versus others (rs3766355, CC vs. AA + AC [P = 0.019; OR, 3.48]). There was also a significant association in low responders versus medium responders versus high responders in rs3753380 (CC vs. CT + TT, P = 0.030). No significant differences were observed between the categories and frequencies of alleles or genotypes of the other 8 SNPs (data not shown).

Reporter Assay of the Prostaglandin $F_{2\alpha}$ Receptor Gene

Because there were associations between the genotypes of 2 SNPs (rs3753380 and rs3766355) and response to latanoprost, we estimated the haplotype frequency of these 2 SNPs and 2 adjacent SNPs, rs3766354 and rs3766353. Of the 2^4 (16) possible combinations of these SNPs, only 6 haplotypes were found by expectation–maximization algorithm analysis. Furthermore,

Table 4. Association Analyses of rs3753380 and rs3766355 with Response to Latanoprost

	Allele	Genotype			
	C:T	CC:CT + TT		TT:CC + CT	
rs3753380 Groups Compared	χ^2 (P)	χ^2 (P)	*Odds Ratio (95% CI)*	χ^2 (P)	*Odds Ratio (95% CI)*
Low responders vs. medium responders vs. high responders	5.20 (0.074)	7.00 (0.030)			
Low responders vs. others	3.37 (0.066)	2.16 (0.14)	0.47 (0.17–1.31)	1.37 (0.24)*	3.61 (0.74–17.72)
High responders vs. others	3.13 (0.077)	6.23 (0.013)	3.82 (1.28–11.45)	<0.01 (0.98)*	1.56 (0.28–8.66)
	Allele	**Genotype**			
	A:C	AA:AC + CC		CC:AA + AC	
rs3766355 Groups Compared	χ^2 (P)	χ^2 (P)	*Odds Ratio (95% CI)*	χ^2 (P)	*Odds Ratio (95% CI)*
Low responders vs. medium responders vs. high responders	4.20 (0.12)	5.01 (0.082)			
Low responders vs. others	1.66 (0.20)	0.022 (0.88)	1.09 (0.35–3.40)	5.53 (0.019)	3.48 (1.18–10.22)
High responders vs. others	3.48 (0.062)	4.52 (0.033)	2.95 (1.06–8.22)	0.44 (0.51)*	0.53 (0.14–1.98)

CI = confidence interval.
*Yates correction.

4 of the 6 haplotypes accounted for 95% of the subjects (haplotypes 1–4 in Fig 2).

To explore whether these SNPs had an influence on transcriptional activity of the FP receptor gene, a DNA fragment from the promoter region (−640) to exon 2 (+1655) that contained each of the 4 haplotype combinations was prepared and fused to the firefly luciferase gene. Reporter constructs were introduced into HeLa cells, and the luciferase activity of each was measured. As shown in Figure 2, the relative activity of constructs with haplotypes 3 and 4 was significantly reduced compared with that of constructs with haplotypes 1 and 2.

Discussion

Effect of Intraocular Pressure Reduction by Latanoprost in Normal Subjects

It was reported that baseline IOP had an influence on IOP reduction by latanoprost.[30,31] To reduce this effect, we evaluated the efficacy of latanoprost as a percent IOP reduction. Furthermore, we subtracted the IOP fluctuation of the control eyes from the IOP reduction of the treated eyes at each time point to assess the true pharmacological component of IOP reduction. We also measured IOP at 3 time points and evaluated the %ΔIOP to reduce the possible effect of diurnal IOP variations. The %ΔIOP of all subjects was 18.1±1.0 (mean ± SE), and 19% of subjects were judged as low responders (%ΔIOP<10). Aung et al[1] reported that nonresponders (percent IOP reduction < 15) were 5.4% of all subjects, whereas Scherer[2] reported that nonresponders (percent IOP reduction < 20 or IOP reduction < 5 mmHg) were 25% of all subjects. The difference of the ratio of nonresponders or low responders in these reports may be attributed to differences of study design, including subjects, definition of IOP response, and duration of latanoprost treatment.

Association between Single-Nucleotide Polymorphisms in the Prostaglandin $F_{2\alpha}$ Receptor Gene and Effect of Latanoprost

We found a significant correlation between the rs3753380 SNP and %ΔIOP by latanoprost, whereas the other FP receptor gene SNPs were not associated with %ΔIOP. When subjects were classified by %ΔIOP into low, medium, and high responders, rs3766355 was also associated with a response to latanoprost. The results of the promoter assay showed the association between the C allele at rs3766355 in intron 1 and reduced expression of the FP receptor–luciferase reporter in HeLa cells. Although we did not find a significant correlation between the rs3766355 SNP and %ΔIOP, the result of the reporter assay is consistent with the findings that the presence of the C allele or absence of the A allele is associated with the lower responders to latanoprost. As for rs3753380, the T allele, which is associated with reduced %ΔIOP and lower responders, was found only in haplotype 3, one of the haplotype combinations with low transcriptional activity. Therefore, the C allele of rs3766355 and T allele of rs3753380 may cause reduced response to latanoprost through downregulation of FP receptor gene expression.

Zaragoza et al[27] deduced the binding sites of the transcription factors SP-1, GATA-1, STAT-1, AP-1, NFκB, and NF-IL-6 from the 5′-untranslated region of the FP receptor gene. However, none of these putative binding sites was associated with the rs3753380 and rs3766355 SNPs. In addition to the primary transcription start site, the bovine and rat FP receptor genes have one or two additional transcription start sites in intron 1, which is located upstream of the ATG initiator codon.[32,33] Therefore, it is possible that intron 1 affects transcriptional regulation of the human FP receptor gene, although this is not yet well characterized. The results of the reporter assay support this possibility, although further studies are required to elucidate how the rs3753380 and rs3766355 SNPs affect transcriptional activity of the FP receptor gene. At present, although the molecular mechanism by which the 2 SNPs rs3753380 and rs3766355 reduce IOP response to latanoprost is unclear, analysis of these SNPs may help to predict the degree of response to latanoprost.

Single-Nucleotide Polymorphisms in the Coding Region of the Prostaglandin $F_{2\alpha}$ Receptor Gene

In this study, we have identified 2 new SNPs (A−1294C and A938G) in addition to the 8 known SNPs. Stjernschantz[29] reported 4 SNPs—C63T (T21), C213T (S71), A573G (E191), and A1012G (I338V)—but no polymorphisms of these SNPs were found in our preliminary analysis of 24 subjects. This may be due to different characteristics of the subjects, such as race. One of the new SNPs, A938G, is located adjacent to the seventh transmembrane domain and results in an amino acid substitution (K313R). Mutations in this seventh transmembrane domain region have been shown to significantly affect FP receptor protein function—for example, the R291L mutation abolished ligand binding and localization to the plasma membrane, and the D300Q mutation caused loss of discrimination between prostaglandin $F_{2\alpha}$ and prostaglandin D_2.[34] Although A938G did not correlate with a response to latanoprost, it is possible that this SNP affects other functional aspects of the FP receptor such as ligand binding.

Other Genes

The FP receptor is involved in IOP regulation via a pathway consisting of various proteins, including prostaglandin transporter; fatty acid amide hydrolase, which is responsible for the activation of all prostaglandin prodrugs[35]; FP receptor regulatory protein[36]; and matrix metalloproteinases.[20–22] As a preliminary experiment, we analyzed the correlation between %ΔIOP and polymorphisms that were reported previously: T396A in prostaglandin transporter[37]; P129T in fatty acid amide hydrolase[38]; T277S, N576K, and I837V in FP receptor regulatory protein (NCBI database); −1607 insG in matrix metalloproteinase 1[39]; C-1306T in matrix metalloproteinase 2[40]; −1171 delA in matrix metalloproteinase 3[41]; and C-1562T[42] and CA repeats (−131 to −90) in matrix metalloproteinase 9.[43] However, we found no significant correlation. It remains possible that new SNPs that are associated with IOP reduction by latanoprost will be identified in these genes.

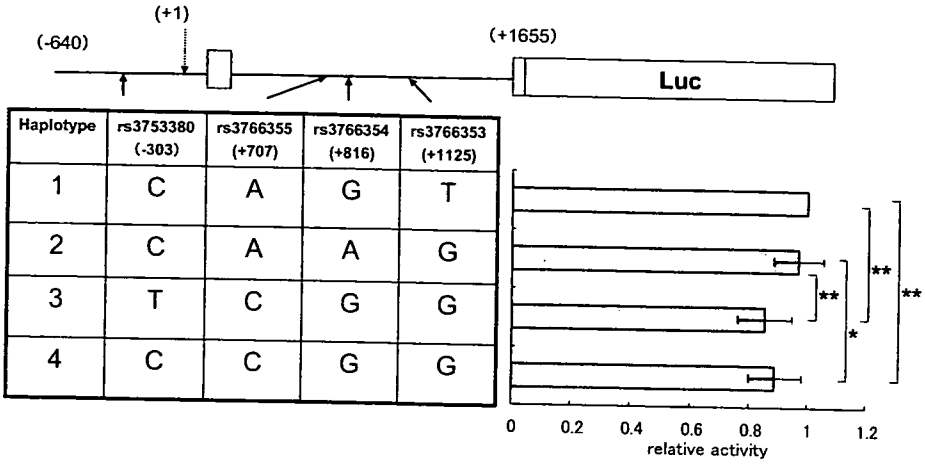

Figure 2. Effects of 4 haplotype combinations of 4 single-nucleotide polymorphisms (SNPs) on the transcriptional activity of the prostaglandin $F_{2\alpha}$ receptor gene. **Top**, Structure of the reporter gene construct and the position of each SNP. Luc = firefly luciferase gene. **Bottom**, The haplotype combination of each clone and relative luciferase activity. Luciferase activity was divided by the activity of renilla to normalize transfection efficiency. Relative activity was calculated with the value of haplotype 1 being 1.0. The values represent means ± standard deviations from 15 independent experiments. Student's *t* tests were performed on paired samples. $^*P<0.02$. $^{**}P<0.01$.

In conclusion, we found an association between 2 SNPs, rs3753380 and rs3766355, in the promoter and intron 1 regions of the FP receptor gene and a short-term latanoprost response in healthy volunteers. The results of the promoter assay suggest that these SNPs downregulate expression of the FP receptor gene, resulting in diminished IOP reduction by latanoprost. Because this study examined only the short-term (1 week) effect of latanoprost in normal subjects, long-term results in patients with glaucoma or ocular hypertension are needed to clarify further the significance of these SNPs in the IOP-lowering effect by latanoprost. Nevertheless, the genotype of these SNPs may be an important determinant of variability in response to latanoprost.

References

1. Aung T, Chew PT, Yip CC, et al. A randomized double-masked crossover study comparing latanoprost 0.005% with unoprostone 0.12% in patients with primary open-angle glaucoma and ocular hypertension. Am J Ophthalmol 2001;131: 636–42.
2. Scherer WJ. A retrospective review of non-responders to latanoprost. J Ocul Pharmacol Ther 2002;18:287–91.
3. Sofowora GG, Dishy V, Muszkat M, et al. A common beta1-adrenergic receptor polymorphism (Arg389Gly) affects blood pressure response to beta-blockade. Clin Pharmacol Ther 2003;73:366–71.
4. Brodde OE, Stein CM. The Gly389Arg beta1-adrenergic receptor polymorphism: a predictor of response to beta-blocker treatment? Clin Pharmacol Ther 2003;74:299–302.
5. Martinez FD, Graves PE, Baldini M, et al. Association between genetic polymorphisms of the beta2-adrenoceptor and response to albuterol in children with and without a history of wheezing. J Clin Invest 1997;100:3184–8.
6. Evans WE, McLeod HL. Pharmacogenomics—drug disposition, drug targets, and side effects. N Engl J Med 2003;348: 538–49.
7. Sasaki M, Oki T, Iuchi A, et al. Relationship between the angiotensin converting enzyme gene polymorphism and the effects of enalapril on left ventricular hypertrophy and impaired diastolic filling in essential hypertension: M-mode and pulsed Doppler echocardiographic studies. J Hypertens 1996;14:1403–8.
8. Baudin B. Angiotensin II receptor polymorphisms in hypertension: pharmacogenomic considerations. Pharmacogenomics 2002;3:65–73.
9. Miller JA, Thai K, Scholey JW. Angiotensin II type 1 receptor gene polymorphism predicts response to losartan and angiotensin II. Kidney Int 1999;56:2173–80.
10. Schwartz SG, Puckett BJ, Allen RC, et al. β_1-adrenergic receptor polymorphisms and clinical efficacy of betaxolol hydrochloride in normal volunteers. Ophthalmology 2005; 112:2131–6.
11. Stjernschantz J, Selen G, Sjoquist B, Resul B. Preclinical pharmacology of latanoprost, a phenyl-substituted PGF2 alpha analogue. Adv Prostaglandin Thromboxane Leukot Res 1995; 23:513–8.
12. Abramovitz M, Boie Y, Nguyen T, et al. Cloning and expression of a cDNA for the human prostanoid FP receptor. J Biol Chem 1994;269:2632–6.
13. Betz R, Lagercrantz J, Kedra D, et al. Genomic structure, 5′ flanking sequences, and precise localization in 1P31.1 of the human prostaglandin F receptor gene. Biochem Biophys Res Commun 1999;254:413–6.
14. Vielhauer GA, Fujino H, Regan JW. Cloning and localization of hFP(S): a six-transmembrane mRNA splice variant of the human FP prostanoid receptor. Arch Biochem Biophys 2004; 421:175–85.
15. Ocklind A, Lake S, Wentzel P, et al. Localization of the prostaglandin F2 alpha receptor messenger RNA and protein in the cynomolgus monkey eye. Invest Ophthalmol Vis Sci 1996;37:716–26.
16. Schlotzer-Schrehardt U, Zenkel M, Nusing RM. Expression and localization of FP and EP prostanoid receptor subtypes in human ocular tissues. Invest Ophthalmol Vis Sci 2002;43: 1475–87.
17. Mukhopadhyay P, Bian L, Yin H, et al. Localization of EP(1) and FP receptors in human ocular tissues by in situ hybridization. Invest Ophthalmol Vis Sci 2001;42:424–8.
18. Watanabe T, Nakao A, Emerling D, et al. Prostaglandin F2 alpha enhances tyrosine phosphorylation and DNA synthe-

sis through phospholipase C-coupled receptor via Ca(2+)-dependent intracellular pathway in NIH-3T3 cells. J Biol Chem 1994;269:17619–25.
19. Sugimoto Y, Hasumoto K, Namba T, et al. Cloning and expression of a cDNA for mouse prostaglandin F receptor. J Biol Chem 1994;269:1356–60.
20. Weinreb RN, Kashiwagi K, Kashiwagi F, et al. Prostaglandins increase matrix metalloproteinase release from human ciliary smooth muscle cells. Invest Ophthalmol Vis Sci 1997;38: 2772–80.
21. Gaton DD, Sagara T, Lindsey JD, et al. Increased matrix metalloproteinases 1, 2, and 3 in the monkey uveoscleral outflow pathway after topical prostaglandin F(2 alpha)-isopropyl ester treatment. Arch Ophthalmol 2001;119: 1165–70.
22. Weinreb RN, Lindsey JD. Metalloproteinase gene transcription in human ciliary muscle cells with latanoprost. Invest Ophthalmol Vis Sci 2002;43:716–22.
23. Lindsey JD, Kashiwagi K, Kashiwagi F, Weinreb RN. Prostaglandins alter extracellular matrix adjacent to human ciliary muscle cells in vitro. Invest Ophthalmol Vis Sci 1997;38: 2214–23.
24. Ocklind A. Effect of latanoprost on the extracellular matrix of the ciliary muscle: a study on cultured cells and tissue sections. Exp Eye Res 1998;67:179–91.
25. Toris CB, Camras CB, Yablonski ME. Effects of PhXA41, a new prostaglandin F2 alpha analog, on aqueous humor dynamics in human eyes. Ophthalmology 1993;100:1297–304.
26. Crowston JG, Lindsey JD, Aihara M, Weinreb RN. Effect of latanoprost on intraocular pressure in mice lacking prostaglandin FP receptor. Invest Ophthalmol Vis Sci 2004;45:3555–9.
27. Zaragoza DB, Wilson R, Eyster K, Olson DM. Cloning and characterization of the promoter region of the human prostaglandin F2alpha receptor gene. Biochim Biophys Acta 2004; 1676:193–202.
28. Excoffier L, Slatkin M. Maximum-likelihood estimation of molecular haplotype frequencies in a diploid population. Mol Biol Evol 1995;12:921–7.
29. Stjernschantz JW. From PGF(2alpha)-isopropyl ester to latanoprost: a review of the development of xalatan. The Proctor Lecture. Invest Ophthalmol Vis Sci 2001;42: 1134–45.
30. Rulo AH, Greve EL, Geijssen HC, Hoyng PF. Reduction of intraocular pressure with treatment of latanoprost once daily in patients with normal-pressure glaucoma. Ophthalmology 1996;103:1276–82.
31. Tamada Y, Taniguchi T, Murase H, et al. Intraocular pressure-lowering efficacy of latanoprost in patients with normal-tension glaucoma or primary open-angle glaucoma. J Ocul Pharmacol Ther 2001;17:19–25.
32. Ezashi T, Sakamoto K, Miwa K, et al. Genomic organization and characterization of the gene encoding bovine prostaglandin F2alpha receptor. Gene 1997;190:271–8.
33. Neuschafer-Rube F, Moller U, Puschel GP. Structure of the 5′-flanking region of the rat prostaglandin F(2alpha) receptor gene and its transcriptional control functions in hepatocytes. Biochem Biophys Res Commun 2000;278:278–85.
34. Neuschafer-Rube F, Engemaier E, Koch S, et al. Identification by site-directed mutagenesis of amino acids contributing to ligand-binding specificity or signal transduction properties of the human FP prostanoid receptor. Biochem J 2003;371: 443–9.
35. Maxey KM, Johnson JL, LaBrecque J. The hydrolysis of bimatoprost in corneal tissue generates a potent prostanoid FP receptor agonist. Surv Ophthalmol 2002;47(suppl):S34–40.
36. Orlicky DJ. Negative regulatory activity of a prostaglandin F2 alpha receptor associated protein (FPRP). Prostaglandins Leukot Essent Fatty Acids 1996;54:247–59.
37. Van Der Zwaag B, Verzijl HT, Beltran-Valero de Bernabe D, et al. Mutation analysis in the candidate Mobius syndrome genes *PGT* and *GATA2* on chromosome 3 and *EGR2* on chromosome 10 [letter online]. J Med Genet 2002;39:E30. Available at http://jmg.bmjjournals.com/cgi/content/full/39/6/e30. Accessed June 30, 2002.
38. Sipe JC, Chiang K, Gerber AL, et al. A missense mutation in human fatty acid amide hydrolase associated with problem drug use. Proc Natl Acad Sci U S A 2002;99:8394–9.
39. Rutter JL, Mitchell TI, Buttice G, et al. A single nucleotide polymorphism in the matrix metalloproteinase-1 promoter creates an Ets binding site and augments transcription. Cancer Res 1998;58:5321–5.
40. Price SJ, Greaves DR, Watkins H. Identification of novel, functional genetic variants in the human matrix metalloproteinase-2 gene: role of Sp1 in allele-specific transcriptional regulation. J Biol Chem 2001;276:7549–58.
41. Ye S, Watts GF, Mandalia S, et al. Preliminary report: genetic variation in the human stromelysin promoter is associated with progression of coronary atherosclerosis. Br Heart J 1995;73: 209–15.
42. Zhang B, Ye S, Herrmann SM, et al. Functional polymorphism in the regulatory region of gelatinase B gene in relation to severity of coronary atherosclerosis. Circulation 1999;99:1788–94.
43. St Jean PL, Zhang XC, Hart BK, et al. Characterization of a dinucleotide repeat in the 92 kDa type IV collagenase gene (*CLG4B*), localization of *CLG4B* to chromosome 20 and the role of *CLG4B* in aortic aneurysmal disease. Ann Hum Genet 1995;59:17–24.